2004

The ACS Virgo Cluster Survey. I. Introduction to the Survey

Patrick Côté
Rutgers University

John P. Blakeslee
The Johns Hopkins University

Laura Ferrarese
Rutgers University

Andrés Jordán
Rutgers University

Simona Mei
Institut d'Astrophysique Spatiale

See next page for additional authors

Authors

Patrick Côté, John P. Blakeslee, Laura Ferrarese, Andrés Jordán, Simona Mei, David Merritt, Miloš Milosavljević, Eric W. Peng, John L. Tonry, and Michael J. West

The ACS Virgo Cluster Survey. I. Introduction to the Survey[1]

Patrick Côté[2], John P. Blakeslee[3], Laura Ferrarese[2], Andrés Jordán[2,4], Simona Mei[5], David Merritt[6], Miloš Milosavljević[7,8], Eric W. Peng[2], John L. Tonry[9], Michael J. West[10]

ABSTRACT

The Virgo Cluster is the dominant mass concentration in the Local Supercluster and the largest collection of elliptical and lenticular galaxies in the nearby universe. In this paper, we present an introduction to the ACS Virgo Cluster Survey: a program to image, in the F475W and F850LP bandpasses ($\approx$ Sloan g and z), 100 early-type galaxies in the Virgo Cluster using the *Advanced Camera for Surveys* on the *Hubble Space Telescope*. We describe the selection of the program galaxies and their ensemble properties, the choice of filters, the field

[1]Based on observations with the NASA/ESA *Hubble Space Telescope* obtained at the Space Telescope Science Institute, which is operated by the association of Universities for Research in Astronomy, Inc., under NASA contract NAS 5-26555.

[2]Department of Physics and Astronomy, Rutgers University, New Brunswick, NJ 08854; pcote@physics.rutgers.edu, lff@physics.rutgers.edu, andresj@physics.rutgers.edu, ericpeng@physics.rutgers.edu

[3]Department of Physics and Astronomy, The Johns Hopkins University, 3400 North Charles Street, Baltimore, MD 21218-2686; jpb@pha.jhu.edu

[4]Claudio Anguita Fellow

[5]Institut d'Astrophysique Spatiale, Université Paris-Sud, Bât. 121, 91405 Orsay, France; simona.mei@ias.u-psud.fr

[6]Department of Physics, Rochester Institute of Technology, 84 Lomb Memorial Drive, Rochester, NY 14623; merritt@mail.rit.edu

[7]Theoretical Astrophysics, California Institute of Technology, Mail Stop 130-33, Pasadena, CA 91125; milos@tapir.caltech.edu

[8]Sherman M. Fairchild Fellow

[9]Institute for Astronomy, University of Hawaii, 2680 Woodlawn Drive, Honolulu, HI 96822; jt@ifa.hawaii.edu

[10]Department of Physics and Astronomy, University of Hawaii, Hilo, HI 96720; westm@hawaii.edu

placement and orientation, the limiting magnitudes of the survey, coordinated parallel observations of 100 "intergalactic" fields with WFPC2, and supporting ground-based spectroscopic observations of the program galaxies. In terms of depth, spatial resolution, sample size and homogeneity, this represents the most comprehensive imaging survey to date of early-type galaxies in a cluster environment. We briefly describe the main scientific goals of the survey which include the measurement of luminosities, metallicities, ages, and structural parameters for the many thousands of globular clusters associated with these galaxies, a high-resolution isophotal analysis of galaxies spanning a factor of ~ 450 in luminosity and sharing a common environment, the measurement of accurate distances for the full sample of galaxies using the method of surface brightness fluctuations, and a determination of the three-dimensional structure of Virgo itself.

Subject headings: galaxies: clusters: individual (Virgo)–galaxies: distances and redshifts–galaxies: ISM: dust–galaxies: elliptical and lenticular–galaxies: nuclei–galaxies: star clusters

1. Introduction

Clusters of galaxies are among the largest gravitationally bound structures in the universe. Although they contain a small fraction of all galaxies in the universe (*e.g.*, Turner & Tyson 1999), they have long provided invaluable constraints on structure formation and galaxy evolution. During the past few decades, it has become abundantly clear that the formation of galaxy clusters is a highly protracted process: most clusters show some degree of substructure (Geller & Beers 1982; Dressler & Shectman 1988; Fitchett & Merritt 1988; Mohr, Fabricant & Geller 1993; Bird 1994) and there is mounting evidence that, even among nearby clusters, the process of virialization may not be fully complete (*e.g.*, Adami, Biviano & Mazure 1998; Drinkwater, Gregg & Colless 2001).

Rich clusters may contain several thousands of member galaxies within a region ~ 1 Mpc in diameter. Collectively, these galaxies usually comprise only a few percent of the total gravitating mass (*e.g.*, Carlberg et al. 1996). Instead, cluster masses are dominated by dark matter, and to a lesser extent, by the X-ray emitting gas which fills their gravitational potential wells (typically $\gtrsim 90\%$ and 10–30% of the total mass, respectively; Böhringer 1995). Yet despite their relatively minor contribution to the cluster mass budget, and to that of the universe in general, much of our understanding of galaxy formation and evolution is based on observations of galaxies in cluster environments.

Virgo is probably the most thoroughly studied cluster of galaxies, being the cluster nearest to our own Galaxy. In most respects, its properties are typical of large clusters. It is a relatively populous system (Abell richness class I; Girardi et al. 1995), consisting of ≈ 2000 cataloged members brighter than $B_T = 18$ (Binggeli, Sandage & Tammann 1987). Mass estimates vary substantially (*e.g.*, 0.15–$1.5 \times 10^{15} M_\odot$; Böhringer et al. 1994; Schindler, Binggeli & Böhringer 1999; McLaughlin 1999a; Tonry et al. 2000; Fouqué et al. 2001), but generally fall within the range typical of rich clusters (Böhringer 1995). It contains vast quantities of X-ray emitting gas (Takano et al. 1989; Böhringer et al. 1994; Schindler et al. 1999), and shows clear evidence for both substructure and non-virialized motions (*e.g.*, Huchra 1985; Binggeli et al. 1987; Binggeli, Popescu & Tammann 1993). Indeed, the property which sets Virgo aside from other clusters is proximity — at a distance of ≈ 17 Mpc (Tonry et al. 2001), it may be studied in a level of detail which will never be possible with more distant systems.

The discovery of the cluster itself dates back to Messier and Méchain, who noted that 13 of the entries in Messier's catalog lie in the constellation of Virgo (Messier 1781).[1] The first systematic studies of the cluster were those of Shapley & Ames (1926; 1929a-e), Hubble & Humason (1931) and Smith (1936). Subsequent studies by Zwicky (1942; 1957) and Holmberg (1958) produced both a better understanding of its spatial structure and a more complete census of cluster members. The cluster richness and its large dynamical mass led de Vaucouleurs (1956; 1961) to identify it as the nucleus of the Local Supercluster. Surveys of the Virgo Cluster culminated in the 1980s, with the heroic efforts of Bruno Binggeli, Allan Sandage and Gustav Tammann (*e.g.*, Binggeli, Sandage & Tammann 1984; 1985; 1987; Sandage, Binggeli & Tammann 1985). Their Virgo Cluster Catalog (VCC) of 2096 galaxies, based on deep photographic images covering an area of ≈ 140 deg^2, still stands as the most complete census of Virgo galaxies brighter than $B_T = 18$.

Continuing studies of Virgo and its constituent galaxies at X-ray (Schindler et al. 1999; Böhringer et al. 2001; Allen et al. 2001), ultraviolet (Lieu et al. 1996; Cortese et al. 2003), optical (Trentham & Hodgkin 2002; Sabatini et al. 2003), infrared (Boselli et al. 1997; Tuffs et al. 2002), and radio (van Driel et al. 2000; Solanes et al. 2002) wavelengths — as well as combinations thereof (Gavazzi et al. 2002; 2003; Boselli, Gavazzi & Sanvito 2003) — have largely confirmed the view of Virgo as an environment that is, in most respects, typical of

---

[1]Messier writes "The constellation Virgo and especially the northern wing is one of the constellations which encloses the most nebulae. This catalog contains 13 which have been determined, viz. Nos. 49, 58, 59, 60, 61, 84, 85, 86, 87, 88, 89, 90 and 91.... Most of these nebulae have been pointed out to me by M. Méchain." It is now recognized that three additional galaxies from Messier's catalog (M98, M99 and M100) are also Virgo members.

rich clusters (see, *e.g.*, Binggeli 1999 and references therein). It therefore seems likely that Virgo will continue to play a central role in the study of galaxy formation and evolution. This is particularly true in the case of early-type galaxies since Virgo contains, by far, the largest collection of early-type giant and dwarf galaxies in the local universe.

Not surprisingly, this enormous reservoir of galaxies has been a favorite target of the *Hubble Space Telescope* (HST) since its launch in 1990. To date, thousands of high-resolution images for fields in Virgo have been obtained with FOC, WFPC, NICMOS, STIS and, especially, WFPC2. The scientific output from the first decade of Virgo research with HST touches upon a remarkably diverse range of astrophysical topics including the extragalactic distance scale, accreting and pulsating stars, the cores of spiral and early-type galaxies, the stellar populations of galaxies, extragalactic globular cluster systems, dwarf galaxies, the nuclear and circumstellar structure of active galaxies, intergalactic stars and diffuse light, the ultraviolet/optical/IR morphologies of nearby galaxies, galaxy collisions and interactions, and pre- and post-main-sequence stages of stellar evolution.

With the installation of the *Advanced Camera for Surveys* (ACS; Ford et al. 1998) during Servicing Mission 3B in March 2002, the imaging capabilities of HST have improved dramatically (*i.e.*, by nearly an order of magnitude in discovery efficiency). Relative to WFPC2, the Wide Field Channel (WFC) mode on ACS boasts a factor of $\sim$ two increase in imaging area and a typical gain of 3–4 times in throughput over the wavelength range 0.4–1.0 μm. ACS thus opens the possibility of obtaining deep, high-resolution optical images for a large sample of Virgo Cluster galaxies in a relatively modest allocation of observing time.

In this paper, the first in a series, we present an introduction to such a program: the ACS Virgo Cluster Survey. The program, which was awarded 100 orbits in Cycle 11, aims to obtain deep F475W ($\approx$ Sloan g) and F850LP ($\approx$ Sloan z) ACS/WFC images for 100 early-type galaxies that are confirmed members of the Virgo Cluster. The paper is organized as follows: we present a brief description of the primary scientific goals of the survey and the anticipated data products in §2, the selection of sample galaxies in §3, and the adopted observing strategy, including choice of filters, exposure times, limiting magnitudes and field placement, in §4. Since the survey also includes supplemental WFPC2 parallel observations of 100 intergalactic fields in Virgo and ground-based, long-slit spectroscopy of the program galaxies, brief descriptions of these observations are given in §5 and §6, respectively. Scientific results from the survey will be presented in future papers in this series.

2.   Motivation

It is clear from the above discussion that high-spatial resolution, multi-color imaging for a large sample of Virgo Cluster galaxies would provide a valuable resource for many different scientific applications. In this section, we give a brief description of three specific scientific programs which have motivated the present survey.

2.1.   Extragalactic Globular Cluster Systems

Globular clusters (GCs) are attractive diagnostics of galaxy formation and evolution for several reasons. They are ubiquitous, found in association with galaxies of all type spanning a factor of $\sim 10^4$ in mass. Roughly 0.25% of the total baryonic mass in galaxies (*i.e.*, gas and stars) takes the form of GCs (McLaughlin 1999b), meaning that the most luminous galaxies may contain many thousands of GCs (*e.g.*, Harris, Pritchet & McClure 1995; Blakeslee et al. 2003). They are the brightest, readily identifiable objects in early-type galaxies, and since they consist of coeval stars with nearly identical metallicities, the interpretation of their broadband colors is much simpler than in composite stellar systems such as their host galaxies.

The metallicity distribution of a given GC system reflects the chemical enrichment history of its parent galaxy (see, *e.g.*, the review of West et al. 2004), while the measurement of GC ages provides a means of reconstructing the likely complex history of mergers and star formation undergone by the galaxy (Cohen, Blakeslee & Ryzhov 1998; Puzia et al. 1999; Jordán et al. 2002; Cohen, Blakeslee & Côté 2003). Because GCs represent dynamical test particles orbiting in the gravitational potential wells of their parent galaxies, it is possible to measure both the GC orbital properties and the distribution of dark matter from their radial velocities (Cohen & Ryzhov 1997; Côté et al. 2001; 2003). The radii and velocities of the GCs provide joint constraints on the form of the gravitational potential and the orbital properties of the GCs themselves (Keenan 1981; Innanen, Harris & Webbink 1983; Bellazzini 2004), while the peak of the GC luminosity function (GCLF) continues to receive attention as a possible standard candle (see the review of Harris 2001). Finally, observations with the *Chandra X-Ray Observatory* have shown that many early-type galaxies are surrounded by numerous low-mass X-ray binaries, roughly half of which are associated with GCs (*e.g.*, Sarazin, Irwin & Bregman 2001; Angelini, Loewenstein & Mushotzky 2001; Maccarone, Kundu & Zepf 2003; Jordán et al. 2004a, hereafter Paper III).

Given their versatility in addressing such a wide variety of astrophysical problems, it is not surprising that considerable effort continues to be devoted to the study of extragalactic

GC systems. HST has played a pivotal role in GC research during the past decade, with important contributions coming from the analysis of archival WFPC2 observations for a few dozen galaxies (*e.g.*, Gebhardt & Kissler-Patig 1999; Kundu & Whitmore 2001; Larsen et al. 2001). For the most part, the images used in these studies were planned with other scientific goals in mind, so that the choice of filters, field placement, exposure times, dither patterns, etc., were not optimized for the study of GCs. Perhaps inevitably, such archival observations are somewhat heterogeneous in nature, whereas certain scientific questions (for example, the usefulness of the GCLF as a standard candle) are better addressed with extremely homogeneous datasets.

The ACS Virgo Cluster Survey has been designed to produce the largest, most homogeneous catalog of extragalactic GCs yet assembled. Deep ACS images in F475W and F850LP (see §4) will probe the brightest $\sim 90\%$ of the GCLF in our 100 program galaxies, yielding a sample of $\approx 13,000$ GCs. For individual GCs, measured properties include coordinates, magnitudes, colors, metallicities, and structural parameters (*i.e.*, half-light radius and King concentration index). The high sensitivity and high spatial resolution of HST/ACS are essential since the clusters are both faint and compact. For instance, the GCLF has a apparently universal, roughly Gaussian form (Harris 2001), meaning that the GCLFs of Virgo Cluster galaxies are expected to peak near $g_{475} \sim 24.2$ and $z_{850} \sim 23.0$.[2] At the distance of Virgo, $1''$ corresponds to a projected distance of 82 ± 6 pc (Tonry et al. 2001), so the typical half-light radius of Galactic GCs ($r_h \simeq 3$pc; van den Bergh 1994) translates to slightly less than one ACS/WFC pixel. Thus, while the measurement of GC structural parameters at the distance of Virgo is certainly feasible (*e.g.*, Larsen et al. 2001; Paper III), it is nevertheless challenging, even with excellent spatial resolution afforded by HST.

Future papers in this series will examine the properties of GCs in the program galaxies. First results are presented in Paper III, which examines the connection between low-mass X-ray binaries and GCs in VCC1316 (= M87) using the ACS images and ACIS observations from *Chandra*.

2.2. The Inner Structure of Early-Type Galaxies

Surface photometry and isophotal studies have long provided clues to the origin and structure of early-type galaxies (see Kormendy & Djorgovski 1989 for a review). Yet until the launch of HST, the central regions of these galaxies remained entirely unexplored, being unresolved in ground-based studies with seeing of $\sim 1''$. The first, high-resolution glimpse

---

[2]All g_{475} and z_{850} magnitudes are on the AB system (Fukugita et al. 1996).

into inner regions of early-type galaxies was that of Jaffe et al. (1994), who used WFPC to obtain the V-band images of 14 E and E/S0 galaxies in Virgo. van den Bosch et al. (1994) carried out an isophotal analysis for these galaxies, finding evidence for both significant quantities of dust and embedded stellar disks. Major and minor-axis surface brightness profiles for these galaxies were presented by Ferrarese et al. (1994), who classified them into two categories based on the slope of their central brightness profiles. Similar conclusions were later reached by Lauer et al. (1995) using V-band HST images for 45 early-type galaxies with distances in the range $3 - 280$ Mpc.

The discovery of gas, dust and embedded stellar disks in the cores of these galaxies (see Tran et al. 2001 and references therein) has prompted a rethinking of the traditional view of early-type galaxies as smooth, uniformly-old stellar systems. It is now well established that both the central surface brightness profile and the isophotal structure of a given galaxy reflect its merger history and/or the presence of a central supermassive black hole (Ebisuzaki et al. 1991; Quinlan & Hernquist 1997; Faber et al. 1997). The first attempts to model quantitatively the evolution in central surface brightness during galaxy mergers that involve supermassive black hole binaries have been presented in Milosavljević & Merritt (2001). Using structural parameters derived from HST imaging, Ravindranath, Ho & Filippenko (2002) and Milosavljević et al. (2002) showed the predictions of these binary black hole merger models are broadly consistent with observations.

However, there are reasons to believe that the picture is far from complete. Recent suggestions that the manifold of early-type galaxies can be neatly divided into two families according to the central slope, γ, of their luminosity profiles (*i.e.*, "core" versus "power law" galaxies) have been called into question. For instance, Rest et al. (2001) present results from the largest imaging survey of early-type galaxies conducted to date, consisting of R-band WFPC2 images for 67 galaxies over the range $6 - 54$ Mpc. They find a class of intermediate luminosity galaxies whose luminosity profiles cannot be classified unambiguously as either cores or power laws. Similar conclusions were found by Ravindranath et al. (2001), who used NICMOS imaging to examine the brightness profiles of Lauer et al. (1995) in the H-band, where the effects of dust extinction are minimized. In addition, Graham et al. (2003) have examined in detail the so-called "Nuker Law" parameterization used by Lauer et al. (1995) to model the brightness profiles of their galaxies. This particular model provides an adequate representation of galaxy brightness profiles having limited radial extent (i.e., the WFPC2 brightness profiles published by Lauer et al. typically extent to $\lesssim 10''$), but fails to reproduce the curvature exhibited by the surface brightness profiles of real galaxies over $\sim$ two or more decades in radius. Thus, Graham et al. (2003) find that the very classification of certain galaxies as power laws may be inappropriate, and argue that generalized Sersic models better represent the brightness profiles of real galaxies.

Virgo contains an enormous collection of early-type galaxies which, lying at a nearly identical distance and spanning a wide range in luminosity and mass, offer attractive targets for imaging with ACS. At a distance of only ~ 17 Mpc, structures with physical sizes of ~ 10 pc are resolved directly with ACS/WFC. In addition, ACS/WFC enjoys a tremendous increase in field size relative to WFPC2, so it is possible, at least for the brightest galaxies, to measure brightness profiles out to radii of $\sim 140''$ (≈ 11 kpc) in a single pointing. And since the galaxies themselves lie nearly at the same distance (see §2.3), distance errors and biases due to varying spatial sampling are greatly reduced.

In future papers in this series, we will present F475W and F850LP luminosity profiles for each of the 100 galaxies which comprise the ACS survey. In addition, we will examine their color profiles and isophotal structure, search for the presence of embedded stellar disks, and examine their dust properties. In terms of sample size, this survey exceeds those of Lauer et al. (1995) and Rest et al. (2001), and is the first systematic study of the inner regions of early-type galaxies to include color information.

2.3. The Extragalactic Distance Scale

Virgo is a complex, irregular cluster with a diameter of $\approx 10°$. The spatial distribution of known or suspected members, when combined with radial velocity measurements for the brightest galaxies, reveals that the cluster is, in fact, an aggregate of at least three distinct subsystems associated with M87, M49 and M86 (VCC1316, VCC1226 and VCC881, respectively). The structure of the cluster along the line of sight remains a matter of debate, with estimates of the back-to-front depth ranging from ± 6–8 Mpc (Young & Currie 1995; Yasuda, Fukugita & Okamura 1997) to ± 2 (Neilsen & Tsvetanov 2000). In principle, if accurate distances for a large sample of early-type cluster members were available, it would be possible not only to measure the cluster depth, but to map out its full three-dimensional structure. Such information would be useful in refining the calibration of various far-field Pop II distance indicators (*e.g.*, Tully-Fisher, fundamental plane), aiding in the interpretation of the cluster velocity field and mass modeling, and characterizing the intrinsic dispersion of those distance indicators which have been applied to multiple Virgo members.

Of the possible distance indicators, the method of surface brightness fluctuations (SBF) seems best suited to the task (Tonry & Schneider 1988; Blakeslee, Ajhar & Tonry 1999). This method, in which distances are estimated from the ratio of the second and first moments of their stellar luminosity functions, is both efficient and accurate (with random errors of $\lesssim$ 1.5 Mpc at the distance of Virgo; Tonry et al. 2001). Equally important, it well suited to the measurement of distances for early-type galaxies, including dwarfs. This latter issue is

important since the early-type dwarf galaxies in Virgo are the only class of galaxies which are available in large numbers throughout the cluster, including its core (Binggeli et al. 1985).

SBF distances (derived from V and I images) have now been measured for roughly two dozen giant ellipticals in Virgo (Neilsen & Tsvetanov 2000; Tonry et al. 2001). Recently, B and R images have been been used to measure SBF distances for a sample of 16 dwarf ellipticals in Virgo (Jerjen, Binggeli & Barazza 2004). Despite the small samples, these studies make it clear that Virgo exhibits significant structure along the line of sight. For example, working from the SBF catalog of Tonry et al. (2001), West & Blakeslee (2000) were able to show that the brightest Virgo ellipticals fall along an axis which passes roughly through M87 and M84: the cluster's so-called "principal axis". In a similar vein, Jerjen et al. (2004) find evidence from their sample of dwarf ellipticals for two subclumps at distances of 15.8 and 18.5 Mpc, associated with M87 and M86, respectively.

A key science goal of the ACS Virgo Cluster Survey is the measurement of SBF distances for a large sample of Virgo galaxies. The rationale behind the choice of filters for this component of the survey is given in §4.1. Technical details on the calibration of the z-band SBF method, the procedures used in measuring fluctuation magnitudes from ACS images, and the scientific results on the extragalactic distance scale (*e.g.*, Virgo's three-dimensional structure, a galaxy-by-galaxy comparison SBF and GCLF distances, etc.) will be presented in future papers in this series.

3. Sample Selection: Membership, Spatial Distribution and Luminosities

The most complete and homogeneous survey of galaxies in the Virgo Cluster remains that of Binggeli et al. (1987) who used wide-field photographic blue plates to identify and study galaxies within $\approx 6°$ of the cluster center (defined by M87 = VCC1316). Their Virgo Cluster Catalog (VCC) consists of 2096 galaxies within this ≈ 140 deg^2 region. Membership in the cluster was established through a combination of morphological classifications (*i.e.*, members were identified on the basis of the relation between apparent magnitude and surface brightness) and radial velocity measurements[3] (taken principally from the Virgo Cluster redshift survey; Huchra 1985). In addition to membership classifications and radial velocities, Binggeli et al. (1987) give coordinates, total magnitudes (B_T), and morphologies for each of their VCC galaxies.

---

[3]For some late-type galaxies, cluster membership could also be established through the resolution of star forming knots.

A total of 1277 VCC galaxies were considered by Binggeli et al. (1987) to be members of Virgo; an additional 574 galaxies were listed as possible cluster members (1851 galaxies in total). At the time of its preparation, the VCC contained radial velocities for 403 cluster members. Of these, 352 galaxies have $B_T < 16$, which we take as the faint-end cutoff of the ACS Virgo Cluster Survey. Early-type galaxies were selected from this sample using the VCC morphological classifications of Binggeli & Sandage (1984). Specifically, program galaxies were required to have morphological types of E, S0, dE, dE,N, dS0 or dS0,N. This leaves a total of 163 galaxies.

Due to the limited number of orbits awarded by the time allocation committee, a subset of 100 galaxies were then selected for observation with ACS. The 63 galaxies which were discarded include 13 dwarfs that were previously observed with WFPC2 as part of programs G0-5999, GO-6352 and GO-8600. The remaining galaxies were omitted for a variety of reasons, such as uncertain morphologies, the lack of a clearly visible bulge component, the presence of strong dust lanes, or signs of strong tidal interactions.

In the time since the VCC was compiled, Virgo has been the subject of numerous spectroscopic surveys. As a result, radial velocities are now available for many additional galaxies (*e.g.*, Binggeli, Popescu & Tammann 1993; Drinkwater et al. 1996). According to NED, 897 of the 1851 galaxies originally classified by Binggeli et al. (1987) as certain or possible members of Virgo now have published radial velocities. The upper histogram in Figure 1 shows the distribution of radial velocities for these 897 galaxies, based on the latest NED data. For comparison, the filled histogram shows the distribution of radial velocities for ACS Virgo Cluster Survey galaxies. It is clear that the velocity distribution for the ACSVCS program galaxies closely resembles that of the entire Virgo sample.

The irregular structure of the cluster is apparent in Figure 2, which shows the distribution of 1726 VCC members or possible members on the sky (black circles). This is somewhat fewer than the 1851 members or possible members listed in the VCC since we show only those galaxies that have $\delta_{\mathrm{B1950}} \geq 5°$, meaning that they are not associated with the Southern Extension of Virgo (Sandage et al. 1985). For comparison, the red symbols show the 100 galaxies from the ACS Virgo Cluster Survey, which fall in the declination range $7°.2 \leq \delta_{\mathrm{B1950}} \leq 18°.2$.

Sandage et al. (1985) examined the luminosity function of Virgo Cluster galaxies in detail, including its dependence on morphology. Numerous subsequent studies have used more sensitive photographic plates (*e.g.*, Impey, Bothun & Malin 1988; Phillipps et al. 1998) or wide-field CCD mosaic cameras (Trentham & Hodgkin 2002; Sabatini et al. 2003) to explore the faint-end behavior of the Virgo luminosity function and to search for bright galaxies with compact sizes or extreme surface brightnesses which might have gone undetected by Sandage

et al. (1985). While the precise form of the faint-end of the Virgo luminosity function remains a matter of debate, the various surveys generally agree on a high level of completeness of the VCC for $B_T \lesssim 18$, the completeness limit estimated by Binggeli et al. (1987).

The upper panel of Figure 3 shows the luminosity function of 956 early-type galaxies judged by Binggeli et al. (1987) to be members of Virgo. The lower panel of this figure shows the same luminosity function in logarithmic form. The filled histogram (upper panel) and filled circles (lower panel) show the corresponding luminosity functions for the ACS Virgo Cluster Survey program galaxies, which have $9.31 \leq B_T \leq 15.97$ (corresponding to a factor of ~ 450 in luminosity). Note that these galaxies are all considerably brighter than the VCC completeness limit of $B_T \approx 18$ (indicated by the arrows in Figure 3). The inset in the upper panel of this figure shows the completeness of the ACS Virgo Cluster Survey as a function of magnitude — the dotted curve shows the completeness in 0.5 mag bins, while the dashed curve shows the variation in cumulative completeness. The final sample of galaxies constitutes a complete sample of early-type members of the Virgo Cluster with $B_T < 12$. Brighter than $B_T \simeq 16$, the survey includes 44% of the early-type members of Virgo.

General properties for the program galaxies are given in Table 1. From left to right, this table records the magnitude ranking from $1-100$ (which also serves as the identification number for each galaxy in the survey), VCC number, right ascension and declination, blue magnitude, heliocentric radial velocity from NED, morphological type from NED, and alternative names in the Messier, NGC, UGC or IC catalogs. Table 2 gives the breakdown of this sample in terms of morphology; roughly two thirds of the galaxies in the survey (65 objects) are elliptical (E) or lenticular (S0) galaxies. The remaining third of the sample (35 objects) are dwarfs of type dE, dE,N, or dS0.

4. Observational Strategy

The observing strategy adopted for the ACS Virgo Cluster Survey was chosen with the scientific goals from §2 in mind. Critical issues in planning the observing program include the selection of program galaxies (discussed in §3), and the choice of filters, exposure times and field orientation. These issues are discussed in detail below.

4.1. Choice of Filters

Two filters are required since color information is an essential ingredient in all three science programs. That is to say, multi-wavelength imaging is needed to select GC candidates

and to estimate their metallicities, measure color profiles for the galaxies and examine their dust properties, and to quantify the stellar population dependence of the SBF magnitudes. The choice of filters is driven by the desire for high-throughput and the need for exceptional metallicity and age sensitivity when modeling the underlying stellar populations.

The F475W and F850LP filters, which offer a combination of high throughput and excellent age and metallicity sensitivity, are equivalent to the g and z filters in the Sloan Digitized Sky Survey system. Transmission curves for the two filters are shown in Figure 4, which also includes a comparison to the F555W ($\approx V$) and F814W ($\approx I$) filters on WFPC2. This latter filter/camera combination is the most commonly used in previous HST studies of extragalactic GC systems and SBF measurements (*e.g.*, Gebhardt & Kissler-Patig 1999; Kundu & Whitmore 2001; Larsen et al. 2001; Ajhar et al. 1997; Neilsen & Tsvetanov 2000). The throughput advantage of F475W and F850LP on the ACS relative to F555W and F814W on WFPC2 is a factor of 2–4, with an increase in color baseline of $\approx 50\%$.

Figures 5 and 6 show the predicted age and metallicity sensitivity of this filter combination based on the population synthesis models of Bruzual & Charlot (2003), assuming a Salpeter IMF. The magnitudes and colors shown here were determined using the F475W and F850LP filter transmission curves of Sirianni et al. (2004; private communication). Figure 5 shows the behavior, in the g_{475} versus $(g_{475} - z_{850})$ plane, of simple stellar population models normalized to a total mass of $\mathcal{M} = 2.4 \times 10^5 \mathcal{M}_\odot$ (appropriate for the mean mass of the Galactic GCs; McLaughlin 1999b). The time evolution in $(g_{475} - z_{850})$ color of these model stellar populations over the age range 100 Myr $\leq$ T $\leq$ 15 Gyr is shown in Figure 6. If we approximate the behavior by linear relations between age and color, then a least-squares fit to the model predictions in Figure 6 gives

$$0.57 \lesssim \frac{\partial(g_{475} - z_{850})}{\partial \log \mathrm{T}} \lesssim 0.91 \text{ mag dex}^{-1}$$

for metallicities between $-2.25 \lesssim$ [Fe/H] $\lesssim +0.56$ dex. The corresponding dependence in $(V - I)$ color is $0.33 - 0.51$ mag dex^{-1}. For comparison, the metallicity sensitivity of the $(g_{475} - z_{850})$ index at a constant age of 10 Gyr is,

$$\frac{\partial(g_{475} - z_{850})}{\partial[\mathrm{Fe/H}]} \simeq 0.36 \text{ mag dex}^{-1},$$

or twice that of $(V - I)$, which has slope $\simeq 0.18$ mag dex^{-1}.

This filter combination is also advantageous when trying to determine the incidence of dust in the target galaxies. Being bluer, dust absorption in g_{475} is 0.16 mag larger than in V, assuming a standard reddening law (Cardelli, Clayton & Mathis 1989). In addition, the longer wavelength baseline of the $(g_{475} - z_{850})$ color, compared to the more commonly

adopted $(V - I)$ color, results in a 50% increase in the contrast produced in the color images by a given amount of dust obscuration.

Since a primary goal of the survey is the measurement of accurate SBF distances, this has also driven the choice of filters. A number of considerations suggest that, in general, the z band is a logical choice for SBF studies. Because the SBF signal in early-type galaxies is dominated by evolved stars, the fluctuations are quite red (having typical colors of $\overline{V}$-$\overline{I} \sim$ 2.4; Ajhar & Tonry 1994). Figure 7 compares fluctuation magnitudes, $\overline{M}$, in V, R, I and z_{850} predicted by the models of Blakeslee, Vazdekis & Ajhar (2001). It is evident that the SBF in z_{850} is not only bright (≈ 0.9 mag brighter than in the I-band) but well behaved, with an rms scatter of only 0.066 mag (compared to 0.093 mag in the I band).[4] In addition, the z band is 20% less affected by dust extinction than the I-band, allowing the optical SBF technique to be pushed to lower Galactic latitudes. A complete discussion of the implementation and calibration of the z-band SBF technique will be presented in a future paper.

4.2. Exposure Times and Limiting Magnitudes

A single orbit with HST was devoted to each galaxy. Target visibility for Virgo is $\sim$ 3200 sec, and a variety of overheads (*e.g.*, guide star acquisitions, filter changes and detector readouts) further limit the usable exposure time. Exposure times in the two filters were set by the requirement that the limiting magnitudes in g_{475} and z_{850} reach roughly equal depths for old, metal-rich stellar populations. For each galaxy, we obtained a pair of exposures totaling 720 sec in F475W and 1120 sec in F850LP, CR-SPLIT to aid in the rejection of cosmic rays. An additional 90 sec exposure in F850LP was also taken for each galaxy, in the event that the galaxy nucleus saturated the detector in the red bandpass.

The limiting magnitude of these images is set not only by the choice of filters and exposure times, but also by the background "sky" level which varies both from galaxy to galaxy and as a function of pixel position for individual galaxies. Accurate results for the true completeness limits and photometric uncertainties require detailed artificial star experiments; the results of such experiments will be presented in a future paper. For the time being, we show in Figure 8 the signal-to-noise ratio, S/N, expected for point sources as a function of total sky brightness, μ_V. Results for the F475W and F850LP filters are shown in the upper and lower panels, respectively. The dashed curves show the S/N for exposure times

---

[4]By this rationale, one might expect the near-infrared to be even better for SBF. However, longward of 1μ, the effects of age and metallicity become non-degenerate on $\overline{M}$, leading to increased scatter in the calibration (Blakeslee, Vazdekis & Ajhar 2001).

of 750s in F475W and 1120s in F850LP. At effective radii of $10''$, the surface brightness of the program galaxies is expected to be $\mu_V \sim 19$ mag arcsec^{-2} or less, so that point-sources brighter than $g_{475} \sim 25.5$ or $z_{850} \sim 23.5$ should be detected with S/N $\gtrsim 10$. In regions of low background, the detection limits are expected to be $g_{475} \sim 26.1$ and $z_{850} \sim 24.8$, meaning that the brightest $\sim 95\%$ of the GCLF lies above the detection threshold.

An automated data reduction pipeline has been written to align and combine the images, perform object detection, and measure object magnitudes, colors and structural parameters. A complete description of this pipeline is given in Jordán et al. (2004b; Paper II).

4.3. Field Placement and Orientation

Coordinates for the nucleus of each galaxy were taken from NED. While the precise centering of the galaxy within the ACS/WFC field is not crucial for the study of the GC systems or the determination of fluctuation magnitudes, it is critical for the measurement of nuclear surface brightness profiles. For instance, "break" radii for the brightest Virgo galaxies can approach several arcseconds (Byun et al. 1995), so it is important that the nuclei be placed well away from the gap between the WFC1 and WFC2 detectors. This is particularly important given the fact that uncertainties in the NED coordinates can approach several arcseconds for a number of the galaxies. For each galaxy, the nucleus was therefore centered on the WFC aperture, which has a reference pixel position at (2096, 200) on the WFC1 detector. For the twelve brightest galaxies, the nucleus was then offset by $10''$ away from the gap using the POS TARG command, giving a distance of $\approx 20''$ between the gap and nucleus. For the remaining galaxies, a POS TARG offset of $5''$ was used, giving a typical gap-nucleus distance of $\approx 15''$.

Figures 9–15 show Digitized Sky Survey images for each of the 100 program galaxies, ranked in order of decreasing blue magnitude. In each panel, an overlay shows the location and orientation of the ACS/WFC field. Final F475W and F850LP images for one program galaxy (VCC1316) are presented in Figure 16, while Figure 17 shows a contour plot for this same galaxy based on the final co-added, background-subtracted F850LP image. The heavy cross marks the location of the WFC aperture, while the arrow shows the direction of the WFPC2 parallel field. For reference, the dashed curve shows the best-fit ellipse at a surface brightness of $\mu_z = 20$ mag arcsec^{-2}.

5. Parallel Observations

The ACS Virgo Cluster Survey includes a significant coordinated parallel component, using WFPC2 to target 100 "blank" fields in Virgo. Since the offset between the WFPC2 and ACS/WFC cameras in the HST focal plane is $\approx 5.'8$ — corresponding to a projected distance of about 29 kpc in Virgo — these fields are effectively "intergalactic" for all but the most luminous galaxies (*i.e.*, the cluster potential exceeds that of the adjacent galaxy).

Deep images in these blank fields are useful for two reasons. First, while the ACS images target the central regions of the program galaxies where the surface density of GCs is highest, accurate measurements of the background surface density of GC contaminants are required for both the statistical removal of background sources from the resulting GC catalogs (a crucial issue for the faintest galaxies since they contain relatively few GCs) and the determination of GC surface density profiles (see Côté et al. 2001 for a demonstration of the problems involved). Second, recent studies of isolated red giant branch stars and planetary nebulae in Virgo (see Durrell et al. 2002 and references therein) suggest that 10–20% of the cluster's total luminosity may reside in a diffuse, intergalactic component. Although red giant branch stars and planetary nebulae in Virgo are much too faint to detect in a single orbit with HST, the detection of any intergalactic GCs (West et al. 1995; Jordán et al. 2003) associated with this diffuse component would be straightforward.[5] Finally, spectroscopic surveys of the Fornax Cluster have produced a number of candidate "ultra-compact dwarfs" (*e.g.*, Phillips et al. 2001; Drinkwater et al. 2003). The depth and high spatial resolution of the WFPC2 images will allow the detection of any such ultra-compact dwarfs which might be present in the Virgo blank fields, and the measurement of their properties (*i.e.*, magnitudes, colors and structural parameters).

While any telescope roll angle would suffice for the ACS/WFC imaging, the precise value is important for the parallel observations. For each galaxy, the Visual Target Tuner was used to align the WFPC2 on regions of the sky free relatively from bright galaxies and/or stars. It is especially important to avoid the former contaminants if one wishes to draw conclusions on the properties of putative intergalactic GCs in Virgo. Images were obtained in two filters, F606W ($\approx V$) and F814W ($\approx I$), having respective exposure times of 700s and 1200s (CR-

---

[5]We may estimate the number of intergalactic GCs as follows. Durrell et al. (2002) find from their study of intergalactic RGB stars that $\approx 15\%$ of Virgo's total luminosity resides in this diffuse component. According to Sandage et al. (19854), the luminosity within a region of radius $6°$ is $L_V = 3.3 \times 10^{12}\, L_{V,\odot}$, where we have scaled their estimate to a distance of 17 Mpc and assumed a mean color of $(B - V) = 0.9$ for the intergalactic light. The luminosity contained within our WFPC2 survey area of 0.16 deg^2 is then $7 \times 10^8\, L_{V,\odot}$. Assuming that we probe the upper 90% of the GCLF and that the diffuse light is characterized by a GC specific frequency of $S_N = 4$, we expect our parallel fields to contain ~ 30 intergalactic GCs.

SPLIT to facilitate the rejection of cosmic rays). For a point-source signal-to-noise ratio of S/N = 10, the expected limiting magnitudes for these images are $V_{\rm lim} \simeq 26.0$ and $I_{\rm lim} \simeq 24.7$. Since these limiting magnitudes are $\Delta V \simeq 2.1$ mag and $\Delta I \simeq 1.9$ mag past the V- and I-band GCLF turnovers in Virgo (Larsen et al. 2001), the parallel observations probe the upper 90–95% of the GCLF in Virgo. More details on the WFPC2 observations and their analysis will be presented in a future paper.

6. Long-slit Spectroscopy

The overarching goal of the ACS Virgo Cluster Survey is an improved understanding of how early-type galaxies form and evolve. To realize the full potential of the HST dataset, it is important to utilize constraints on the dynamics of the galaxies themselves, particularly the internal distribution of gravitating mass. Since the chemical enrichment histories of each galaxy's GC system and underlying stellar populations likely depend on the depth and shape of its gravitational potential well, we initiated a ground-based program to obtain long-slit, integrated-light spectra for each galaxy in the survey. During the 2003 and 2004 observing seasons, spectra were obtained for 95 of the 100 program galaxies using three different instrument/telescope combinations. First, spectra in the range 4000–6000 Å (at an instrumental resolution of $\sigma_{ins} \approx 60$ km s^{-1}) were obtained for galaxies with $B_T \leq 11.8$ using the GoldCam spectrometer on the KPNO 2.1m telescope. Second, galaxies in the range $11.8 < B_T < 14.6$ were observed with the RC spectrograph on the KPNO 4m telescope; two grating configurations were used for these observations, yielding spectra in the range 4200–6200 Å ($\sigma \approx 60$ km s^{-1}) or 4800–5600 Å ($\sigma \approx 35$ km s^{-1}). Finally, galaxies in the range $14.6 \leq B_T \leq 16.0$ were observed using the Echelle Spectrograph and Imager (ESI) on the Keck II 10m telescope; these spectra cover the wavelength range $4000 \lesssim \lambda \lesssim 10,000$ Å with a resolution of $\sigma \approx 30$ km s^{-1}. A complete description of these spectroscopic observations, including the determination of velocity dispersion profiles, rotation curves, mass profiles and line index measurements, will be presented in future papers.

7. Summary

This paper has provided a brief introduction to the ACS Virgo Cluster Survey (GO-9401). In terms of depth, spatial resolution, sample size and homogeneity, this represents the most comprehensive imaging survey to date of early-type galaxies in a cluster environment. Scientific results from the survey will be presented in future papers in this series. More information on the survey, including object catalogs and other data products, are available

from the program website: http://www.physics.rutgers.edu/∼pcote/acs.

REFERENCES

Adami, C., Biviano, A., & Mazure, A. 1998, A&A, 331, 439

Ajhar, E.A. & Tonry, J.L. 1994, ApJ, 429, 557

Ajhar, E.A., Lauer, T.R., Tonry, J.L., & Blakeslee, J.P., Dressler, A., Holtzman, J.A., & Postman, M. 1997, AJ, 114, 626

Allen, S.W., Fabian, A.C., Johnstone, R.M., Arnaud, K.A., & Nulsen, P.E.J. 2001, MNRAS, 322, 589

Angelini, L., Loewenstein, M., & Mushotzky, R.F. 2001, ApJ, 557, 35

Beasley, M.A., Sharples, R.M., Bridges, T.J., Hanes, D.A., Zepf, S.E., Ashman, K.M., & Geisler, D. 2000, MNRAS, 318, 1249

Bellazzini, M. 2004, MNRAS, 347, 119

Binggeli, B., & Sandage, A. 1984, AJ, 89, 919

Binggeli, B., Sandage, A., & Tammann, G.A. 1984, AJ, 89, 64

Binggeli, B., Sandage, A., & Tammann, G.A. 1985, AJ, 90, 1681

Binggeli, B., Tammann, G.A., & Sandage, A. 1987, AJ, 94, 251

Binggeli, B., Popescu, C.C., & Tammann, G.A. 1993, A&AS, 98, 275

Binggeli, B. 1999, in Ringberg Workshop, The Radio Galaxy Messier 87, ed. H.-J. Rser & K. Meisenheimer (Berlin: Springer), 9

Bird, C.M. 1994, AJ, 107, 1637

Blakeslee, J.P., Ajhar, E.A., & Tonry, J.L. 1999, in Post-*Hipparcos* Cosmic Candles, ed. A. Heck & F. Caputo (Boston: Kluwer), 181

Blakeslee, J.P., et al. 2003, in IAU Joint Discussion #6, 34.

Blakeslee, J.P., Vazdekis, A., & Ajhar, E.A. 2001, MNRAS, 320, 193

Böhringer, H., Briel, U.G., Schwarz, R.A., Voges, W., Hartner, G., & Trumper, J. 1994, Nature, 368, 828

Böhringer, H. 1995, Rev. Mod. Astron., 8, 259

Böhringer, H., Belsole, E., Kennea, J., Matsushita, K., Molendi, S., Worrall, D.M., Mushotzky, R.F., Ehle, M., Guainazzi, M., Sakelliou, I., Stewart, G., Vestrand, W.T., & Dos Santos, S. 2001, A&A, 365, 181

Boselli, A., Tuffs, R.J., Gavazzi, G., Hippelein, H., & Pierini, D. 1997, A&AS, 121, 507

Boselli, A., Gavazzi, G., & Sanvito, G. 2003, A&A, 402, 37

Bruzual, G., & Charlot, S. 2003, MNRAS, 344, 1000

Byun, Y.-I.; Grillmair, C.J., Faber, S.M., Ajhar, E.A., & Dressler, A., Kormendy, J., Lauer, T.R., Richstone, D., & Tremaine, S. 1995, AJ, 111, 1889

Cardelli, J.A., Clayton, G.C., & Mathis, J.S. 1989, ApJ, 345, 245

Carlberg, R.G., Yee, H.K.C., Ellingson, E., Abraham, R., Gravel, P., Morris, S., & Pritchet, C.J. 1996, ApJ, 462, 32

Cohen, J.G., & Ryzhov, A. 1997, ApJ, 486, 230

Cohen, J.G., Blakeslee, J.P., & Rhyzov, A. 1998, AJ, 115, 2356

Cohen, J.G., Blakeslee, J.P., & Côté, P. 2003, ApJ, 592, 866

Cortese, L., Gavazzi, G., Boselli, A., Iglesias-Paramo, J., & Donas, J., & Milliard, B. 2003, A&A, 410, 25

Côté, P., McLaughlin, D.E., Hanes, D.A., Bridges, T.J., Geisler, D., Merritt, D., Hesser, J.E., Harris, G.L.H., & Lee, M.G. 2001, ApJ, 559, 828

Côté, P., McLaughlin, D.E., Cohen, J.G., & Blakeslee, J.P. 2003, ApJ, 591, 850

de Vaucouleurs, G. 1956, Vistas in Astron., 2, 1584

de Vaucouleurs, G. 1961, ApJS, 6, 213

Dressler, A., & Schectman, S.A. 1988, AJ, 95, 985

Drinkwater, M.J., Currie, M.J., Young, C.K., Hardy, E., & Yearsley, J.M. 1996 MNRAS, 279, 595

Drinkwater, M.J., Gregg, M.D., & Colless, M.M. 2001, ApJ, 548, L139

Drinkwater, M.J., Gregg, M.D., Hilker, M., Bekki, K., Couch, W.J., Ferguson, H.C., Jones, J.B., & Phillipps, S. 2003, Nature, 423, 519

Durrell, P.R., Ciardullo, R., Feldmeier, J.J., Jacoby, G.H., & Sigurdsson, S. 2002, ApJ, 570, 119

Ebisuzaki, T., Makino, J., & Okumura, S.K. 1991, Nature, 354, 212

Faber, S.M., Tremaine, S., Ajhar, E.A., Byun, Y-I, Dressler, A., Gebhardt, K., Grillmair, C., Kormendy, J., Lauer, T.R., & Richstone, D. 1997, 114, 1771

Ferrarese, L., van den Bosch, F.C., Ford, H.C., Jaffe, W., O'Connell, R.W. 1994, AJ, 108, 1598

Fitchett, M., & Merritt, D. 1988, ApJ, 335, 18

Ford, H.C., et al. 1998, Proc. SPIE, 3356, 234

Fouqué, P., Solanes, J.M., Sanchis, T., & Balkowski, C. 2001, A&A, 375, 770

Fukugita, M., Ichikawa, T., Gunn, J.E., Doi, M., Shimasaku, K., & Schneider, D.P. 1996, AJ, 111, 1748

Gavazzi, G., Bonafanti, C., Sanvito, G., Boselli, A., & Scodeggio, M. 2002, ApJ, 576, 135

Gavazzi, G., Boselli, A., Donati, A., Franzetti, P., & Scodeggio, M. 2003, A&A, 400, 451

Gebhardt, K., & Kissler-Patig, M. 1999, AJ, 118, 1526

Geller, M.J., & Beers, T.C. 1982, PASP, 94, 421

Girardi, M., Biviano, A., Giuricin, G., Mardirossian, F., & Mezzetti, M. 1995, ApJ, 438, 527

Graham, A.W., Erwin, P., Trujillo, I., & Asensio Ramos, A. 2003, AJ, 125, 2951

Harris, W.E., Pritchet, C.J., & McClure, R.D. 1995,

Harris, W.E. 2001, in Star Clusters, Saas-Fee Advanced School 28, ed. L. Labhardt & B. Binggeli (Berlin:Springer), 223

Holmberg, E. 1958, Medn. Lunds. Astr. Obs., 2, 136

Hubble, E., & Humason, M.L. 1931, ApJ, 74, 43

Huchra, J. 1985, in The Virgo Cluster, ESO Workshop proceedings No. 20, ed. O.-G. Richter & B. Binggeli, ESO, Garching, p. 181

Impey, C., Bothun, G., & Malin, D. 1988, ApJ, 330, 634

Innanen, K.A., Harris, W.E., & Webbink, R.F. 1983, AJ, 88, 338

Jaffe, W., Ford, H.C., O'Connell, R.W., van den Bosch, F.C., & Ferrarese, L. 1994, AJ, 108, 1567

Jerjen, H., Binggeli, B., & Barazza F.D. 2004, AJ, 127, 771

Jordán, A., Côté, P., West, M.J., & Marzke, R.O. 2002, ApJ, 576, L113

Jordán, A., West, M.J., Côté, P., & Marzke, R.O. 2003, AJ, 125, 1642

Jordán, A., Côté, P., Ferrarese, L., Blakeslee, J.P., Mei, S., Merritt, D., Milosavljević, M., Peng, E., Tonry, J.L., & West, M.J. 2004a, ApJ, in press (Paper III)

Jordán, A., Blakeslee, J.P., Peng, E., Côté, P., Ferrarese, L., Mei, S., Merritt, D., Milosavljević, M., Tonry, J.L., & West, M.J. 2004b, ApJ, in preparation (Paper II)

Karachentsev, I., & Karachentseva, V. 1982, Soviet Astron. Lett., 8, 104

Keenan, D.W. 1981, A&A, 95, 340

Kormendy, J., & Djorgovski, S.G. 1989, ARA&A, 27, 235

Kundu, A., & Whitmore, B.C. 2001, AJ, 121, 2950

Larsen, S.S., Brodie, J.P., Huchra, J.P., Forbes, D.A., & Grillmair, C.J. 2001, ApJ, 121, 2974

Lauer, T.R., Ajhar, E.A., Byun, Y.-I., Dressler, A., Faber, S.M., Grillmair, C., Kormendy, J., Richstone, D., & Tremaine, S. 1995, AJ, 110, 2622

Lieu, R., Mittaz, J.P.D., Bowyer, S.; Lockman, F.J., & Hwang, C.-Y., & Schmitt, J.H.M.M. 1996, ApJ, 458, L5.

Maccarone, T.J., Kundu, A., & Zepf, S.E. 2003, ApJ, 586, 814

McLaughlin, D.E. 1999a, ApJ, 512, L9

McLaughlin, D.E. 1999b, AJ, 117, 2398

Messier, C. 1781, Connaissance des Temps pour 1784 (Paris), 263.

Milosavljević, M., & Merritt, D. 2001, ApJ, 563,34

Milosavljević, M., Merritt, D., Rest, A., van den Bosch, F.C. 2002, MNRAS, 331, 51

Mohr, J.J., Fabricant, D.G., & Geller, M.J. 1993, ApJ, 413, 492

Neilsen, E.H., & Tsvetanov, Z.I. 2000, ApJ, 536, 255 Grillmair, C., Kormendy, J., Richstone, D., & Tremaine, S. 1995, AJ, 110, 2622

Phillipps, S., Parker, Q.A., Schwartzenberg, J.M., & Jones, J.B. 1998, ApJ, 493, 59

Phillipps, S., Drinkwater, M.J., Gregg, M.D., & Jones, J.B. 2001, ApJ, 560, 201

Puzia, T.H., Kissler-Patig, M., Brodie, J.P., & Huchra, J.P. 1999, AJ, 118, 2734

Quinlan, G.D., & Hernquist, L. 1997, New Astronomy, 2, 533

Ravindranath, S., Ho, L.C., Peng, C.Y., Filippenko, A.V., Sargent, W.L.W. 2001, AJ, 122, 653

Ravindranath, S., Ho, L.C., & Filippenko, A.V. 2002, ApJ, 566, 801

Rest, A., van den Bosch, F.C., Jaffe, W., Tran, H., Tsvetanov, Z., Ford, H.C., Davies, J., Schafer, J. 2001, AJ, 121, 2431

Sabatini, S., Davies, J., Scaramella, R., Smith, R., Baes, M., Linder, S.M., Roberts, S., & Testa, V. 2003, MNRAS, 341, 981

Sandage, A., Binggeli, B., & Tammann, G.A. 1985, AJ, 90, 1759

Sarazin, C.L., Irwin, J.A., & Bregman, J.N. 2001, ApJ, 556, 533

Schindler, S., Binggeli, B., & Böhringer, H. 1999 A&A, 343, 420

Shapley, H. & Ames, A. 1926, Harvard College Observatory Circular, 294

Shapley, H. & Ames, A. 1929, Harvard College Observatory Bulletin, 864

Shapley, H. & Ames, A. 1929, Harvard College Observatory Bulletin, 865

Shapley, H. & Ames, A. 1929, Harvard College Observatory Bulletin, 866

Shapley, H. & Ames, A. 1929, Harvard College Observatory Bulletin, 868

Shapley, H. & Ames, A. 1929, Harvard College Observatory Bulletin, 873

Sirianni, M., et al. 2004, preprint

Smith, S. 1936, ApJ, 83, 23

Solanes, J.M., Sanchis, T., Salvador-Sol, E., Giovanelli, R., & Haynes, M.P. 2002, AJ, 124, 2440

Takano, S., Awaki, H., Koyama, K., Kunieda, H., & Tawara, Y. 1989, Nature, 340, 289

Tonry, J.L., & Schneider, D.P. 1988, AJ, 96, 807

Tonry, J.L., Blakeslee, J.P., Ajhar, E.A., & Dressler, A. 2000, ApJ, 530, 625

Tonry, J.L., Dressler, A., Blakeslee, J.P., Ajhar, E.A., Fletcher, A.B., Luppino, G.A., Metzger, M.R., Moore, C.B. 2001, ApJ, 546, 681

Tran, H.D., Tsvetanov, Z., Ford, H.C., Davies, J., Jaffe, W., van den Bosch, F.C., & Rest, A. 2001, AJ, 121, 2928

Trentham, N., & Hodgkin, S. 2002, MNRAS, 333, 423

Tuffs, R.J., Popescu, C.C., Pierini, D.; Völk, H.J., & Hippelein, H., Leech, K., Metcalfe, L., Heinrichsen, I., & Xu, C. 2002, ApJS, 139, 37

Turner, M.S., & Tyson, J.A. 1999, Rev. Mod. Phys., 71, S145

van den Bergh, S. 1994, AJ, 108, 2145

van den Bosch, F.C.; Ferrarese, L., Jaffe, W., Ford, H.C., & O'Connell, R.W. 1994, AJ, 108, 1579

van Driel, W., Ragaigne, D., Boselli, A., Donas, J., & Gavazzi, G. 2000, A&A, 144, 463

West, M.J., Côté, P., Jones, C., Forman, W., & Marzke, R.O. 1995, ApJ, 453, L77

West, M.J., Côté, P., Marzke, R.O., & Jordán, A. 2004, Nature, 427, 31

West, M.J., & Blakeslee, J.P. 2000, ApJ, 543, 27

Yasuda, N., Fukugita, M., & Okamura, S. 1997, ApJS, 108, 417

Young, C.K., & Currie, M.J. 1995, MNRAS, 273, 1141

Zwicky, F. 1942, ApJ, 95, 555

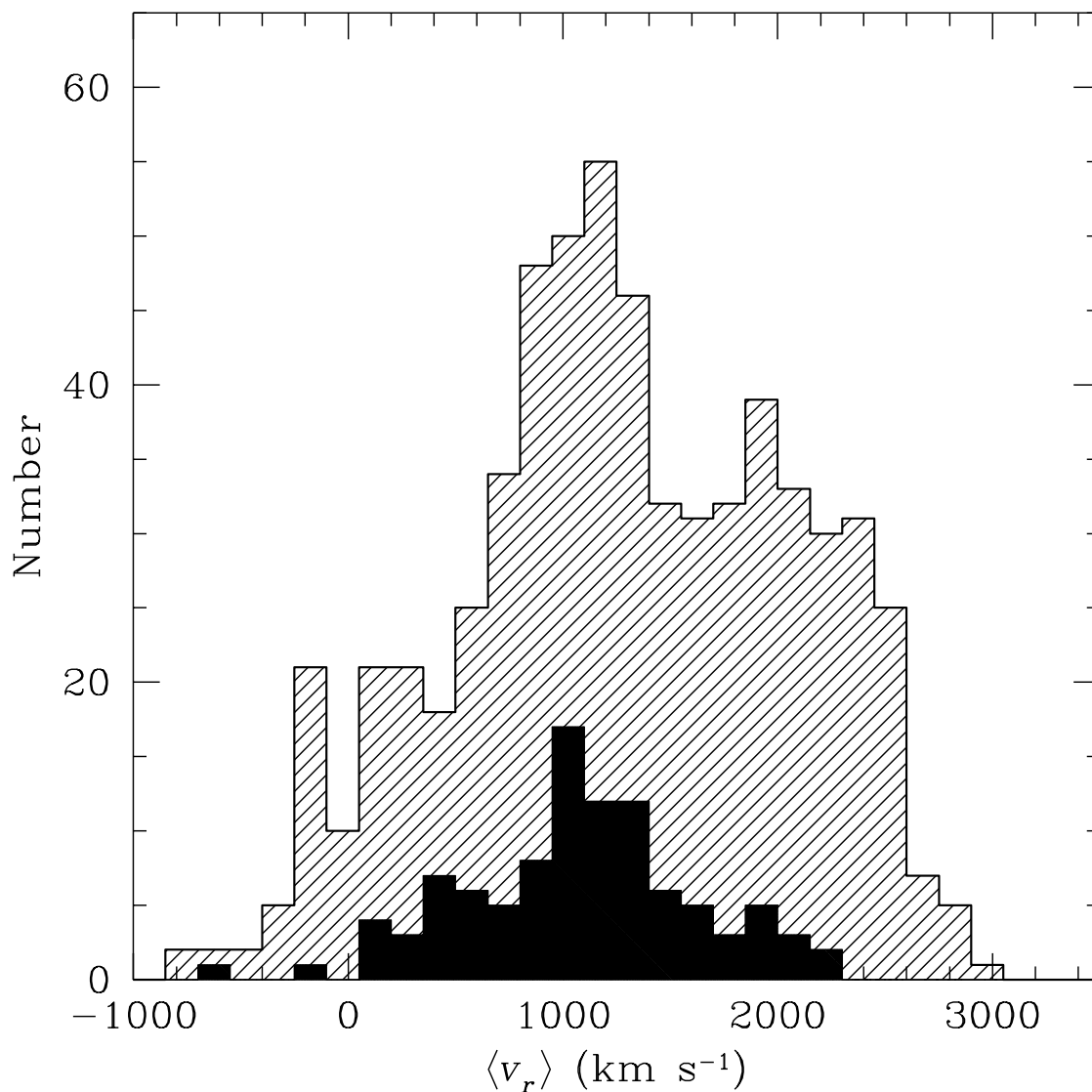Zwicky, F. 1957, Morphological Astronomy (Berlin, Springer Verlag), 71

Fig. 1.— Histogram of radial velocities for 897 galaxies, of all morphological types, classified by Binggeli *et al.* (1987) as members or possible members of the Virgo Cluster *and* having measured radial velocities according to the NASA Extragalactic Database (upper, hatched histogram). The filled lower histogram shows the radial velocity distribution of ACS Virgo Cluster Survey program galaxies.
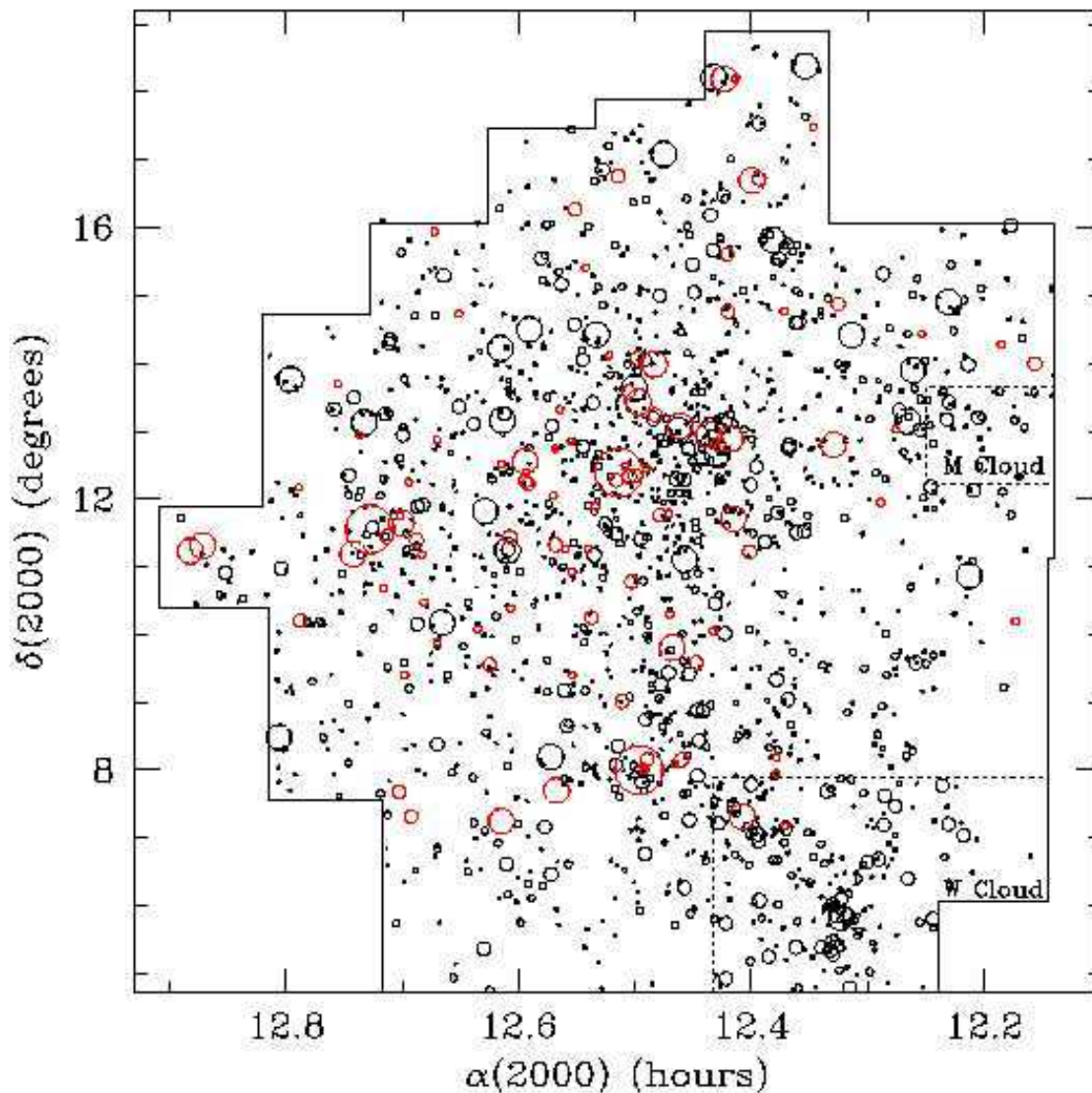
Fig. 2.— Distribution of VCC galaxies on the plane of the sky, adapted from Binggeli *et al*. (1987). The symbol size is proportional to blue luminosity. This figure contains a total of 1726 galaxies, with no restriction on morphological type, that are classified as members or possible members of the Virgo Cluster and have declinations greater than $\delta_{B1950} \simeq 5°$ (meaning that they are not associated with the Southern Extension of Virgo). The M and W Clouds as defined by Sandage *et al*. (1985) are shown by the dotted regions. Red symbols denote the full sample of 100 early-type galaxies from the ACS Virgo Cluster Survey.
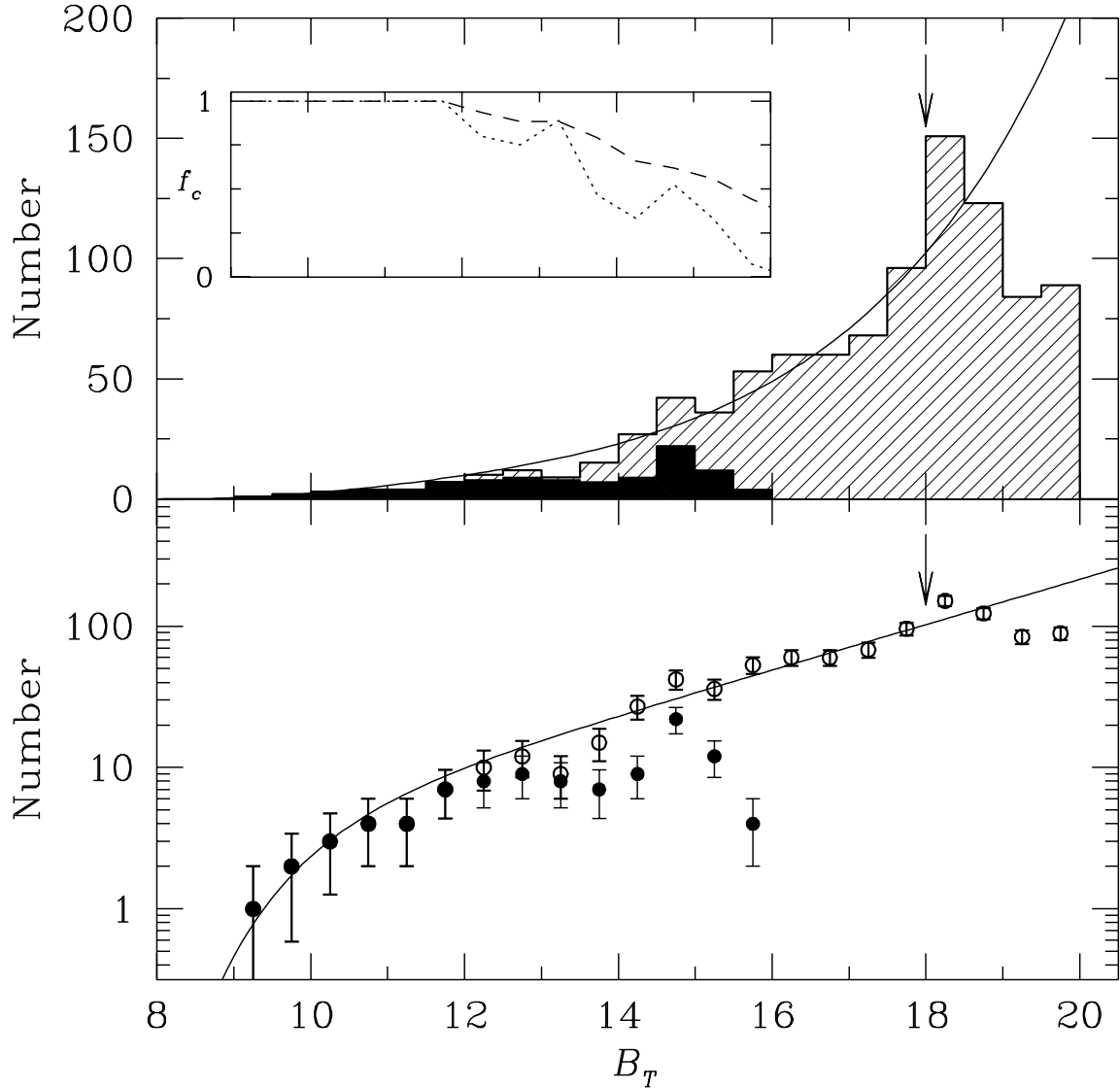
Fig. 3.— *(Upper Panel)* Luminosity function of 956 early-type galaxies ($T \leq 15$) that are classified by Binggeli *et al.* (1987) as members of the Virgo Cluster (upper, hatched histogram). The arrow shows the VCC completeness limit, while the solid curve shows the best-fit Schechter function for E+S0+dE+dS0 galaxies from Sandage *et al.* (1985). The filled lower histogram shows the luminosity function of the 100 early-type galaxies in the ACS Virgo Cluster Survey. *(Inset to Upper Panel)* Differential (dotted curve) and cumulative (dashed curve) completeness fractions for the ACS Virgo Cluster Survey over the range $9 \leq B_T \leq 16$. *(Lower Panel)* Same as above, except in logarithmic form. The open circles show the luminosity function of 956 early-type members of the Virgo Cluster according to Sandage *et al.* (1985). The arrow shows the VCC completeness limit of the original VCC, while the filled circles show the luminosity function of galaxies in the ACS Virgo Cluster Survey. The solid curve is the same as that shown in the upper panel.
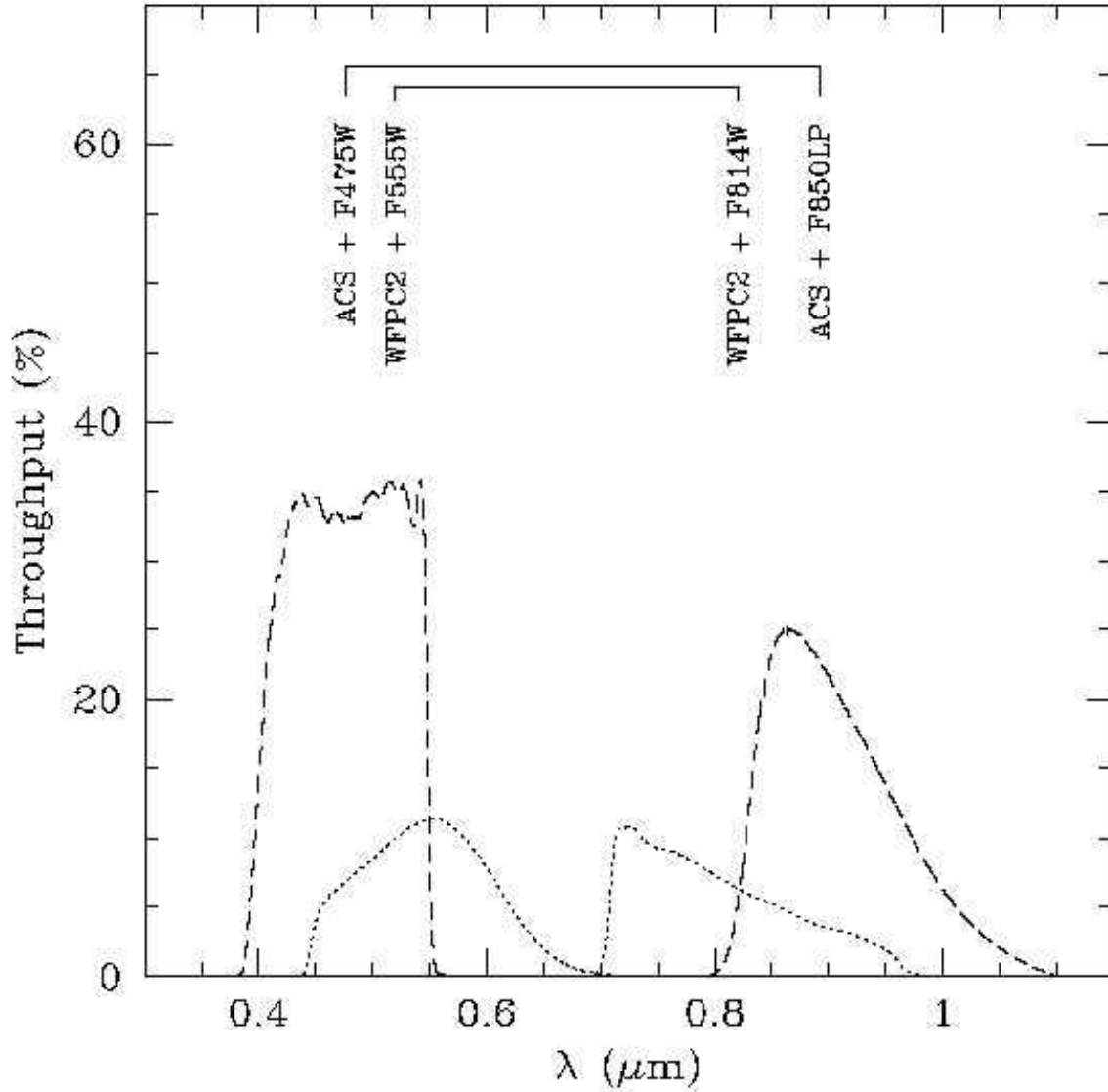
Fig. 4.— Total system throughput for ACS/WFC in the F475W and F850LP bandpasses (dashed curves). For comparison, the dotted curves show the WFPC2 throughput for F555W and F814W, the HST camera/filter combinations used most frequently in the measurement of SBF distances and in studies of extragalactic globular cluster systems.
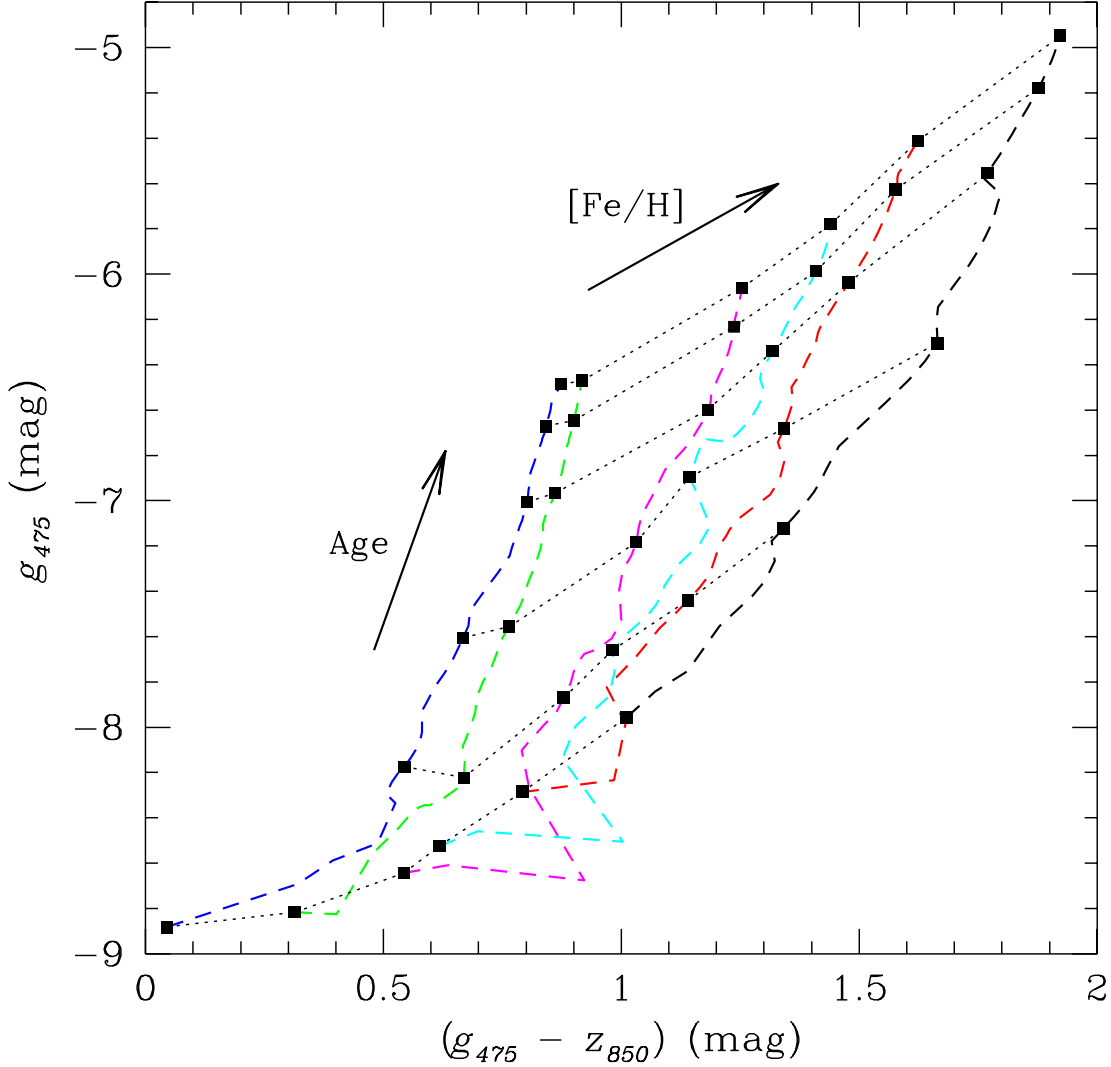
Fig. 5.— Simple stellar populations in the g_{475} versus $(g_{475} - z_{850})$ plane calculated using the population synthesis models of Bruzual & Charlot (2003). The dashed grid lines represent isometallicity tracks of [Fe/H] = –2.25 (blue), –1.65 (green), –0.64 (magenta), –0.33 (cyan), +0.09 (red) and +0.56 (black). The dotted grid lines show isochrones of age T = 1, 2, 4, 8, 12 and 15 Gyr. The g_{475} magnitudes have been scaled to a total mass of $\mathcal{M} = 2.4 \times 10^5 \mathcal{M}_\odot$, the approximate mean mass of globular clusters in the Milky Way.
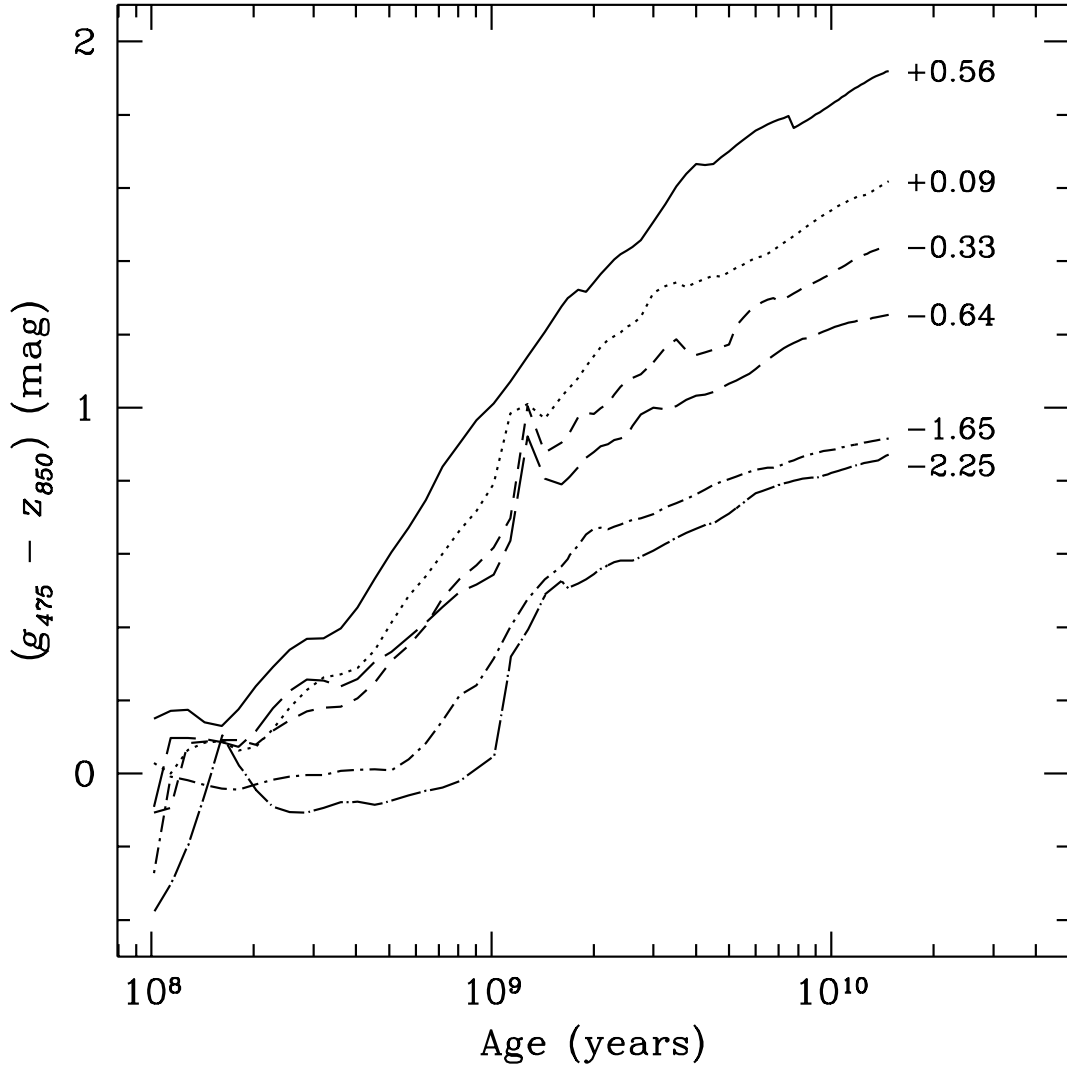
Fig. 6.— Time evolution of $(g_{475} - z_{850})$ color for simple stellar populations calculated using the population synthesis models of Bruzual & Charlot (2003). The curves show isometallicity tracks of [Fe/H] = –2.25, –1.65, –0.64, –0.33, +0.09 and +0.56 dex.
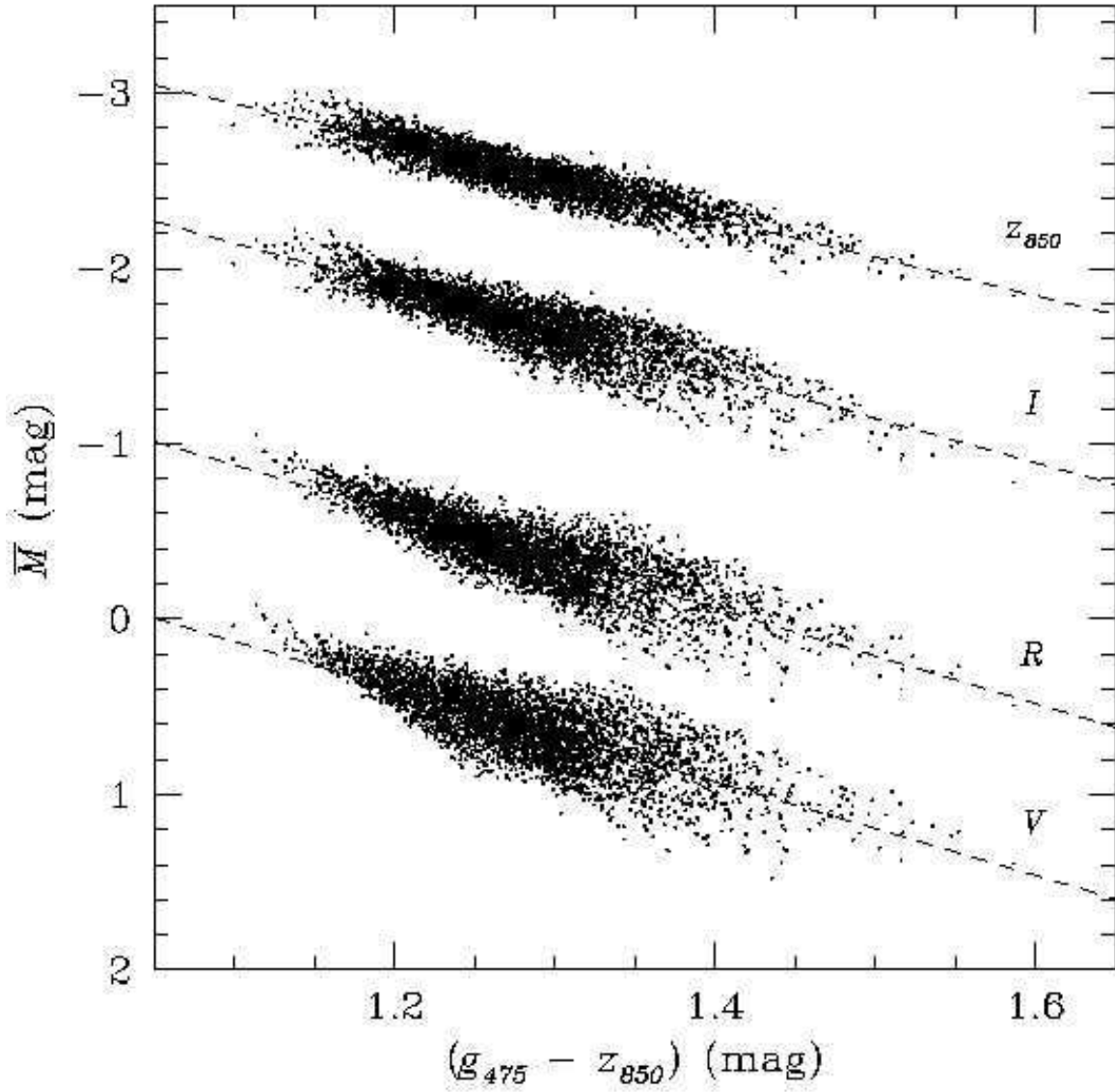
Fig. 7.— Fluctuation magnitude, $\overline{M}$, in V, R, I and z_{850} calculated using the composite stellar population models of Blakeslee, Vazdekis & Ajhar (2001) and transformed to z_{850} via the relations of Fukugita et al. (1996).
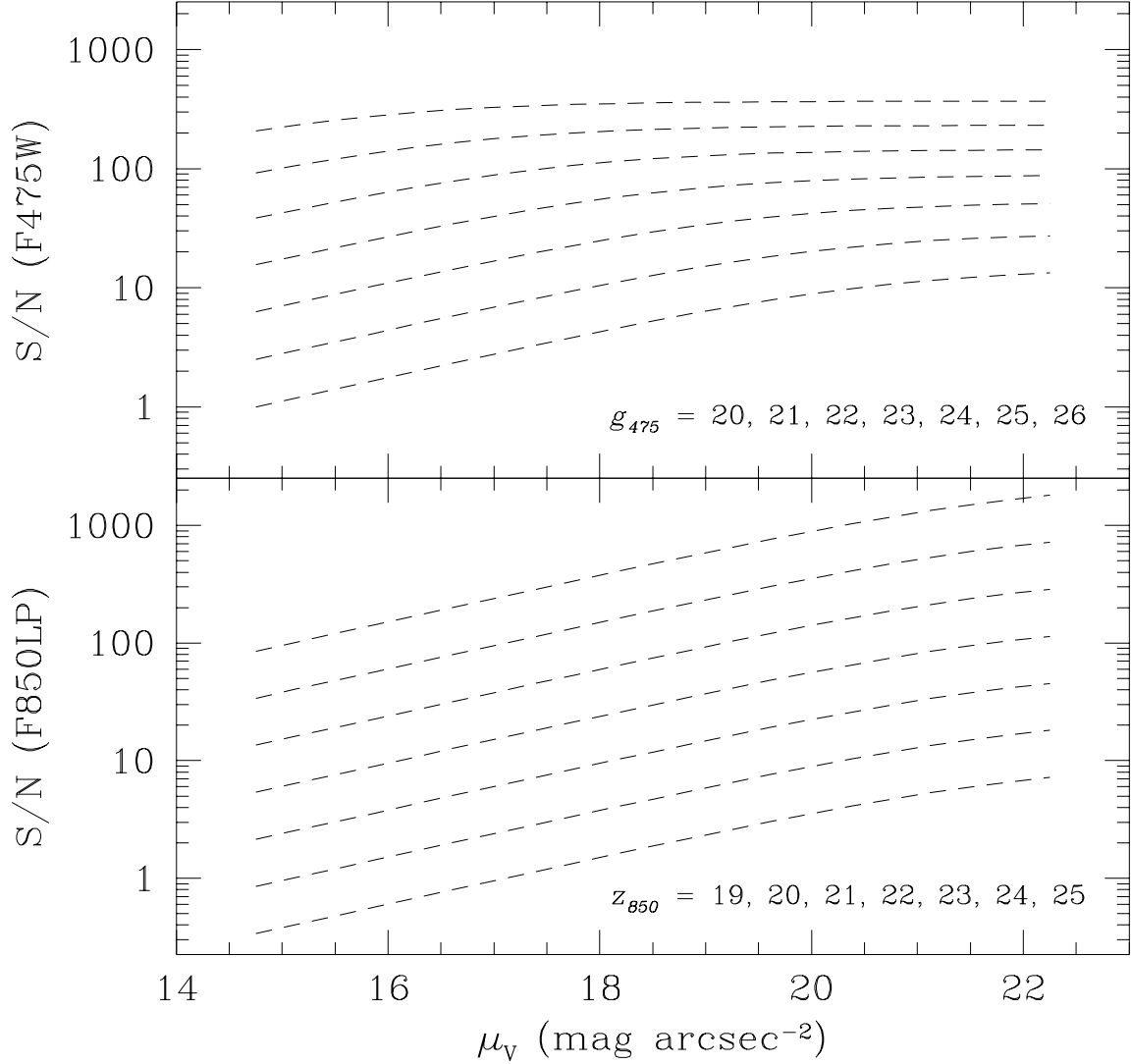
Fig. 8.— *(Upper Panel)* Point-source signal-to-noise ratio, S/N, achieved in a total exposure time of 2×375 = 750 sec in the F475W filter. The signal-to-noise ratio measured in a 3×3 pixel aperture is plotted as a function of the sky brightness, μ_V. From top to bottom, the seven curves correspond to point sources of g_{475} = 20, 21, 22, 23, 24, 25 and 26. *(Lower Panel)* Same as above, except for a total exposure time of 2×560 = 1120 sec in the F850LP filter. From top to bottom, the seven curves correspond to point sources of z_{850} = 19, 20, 21, 22, 23, 24 and 25.
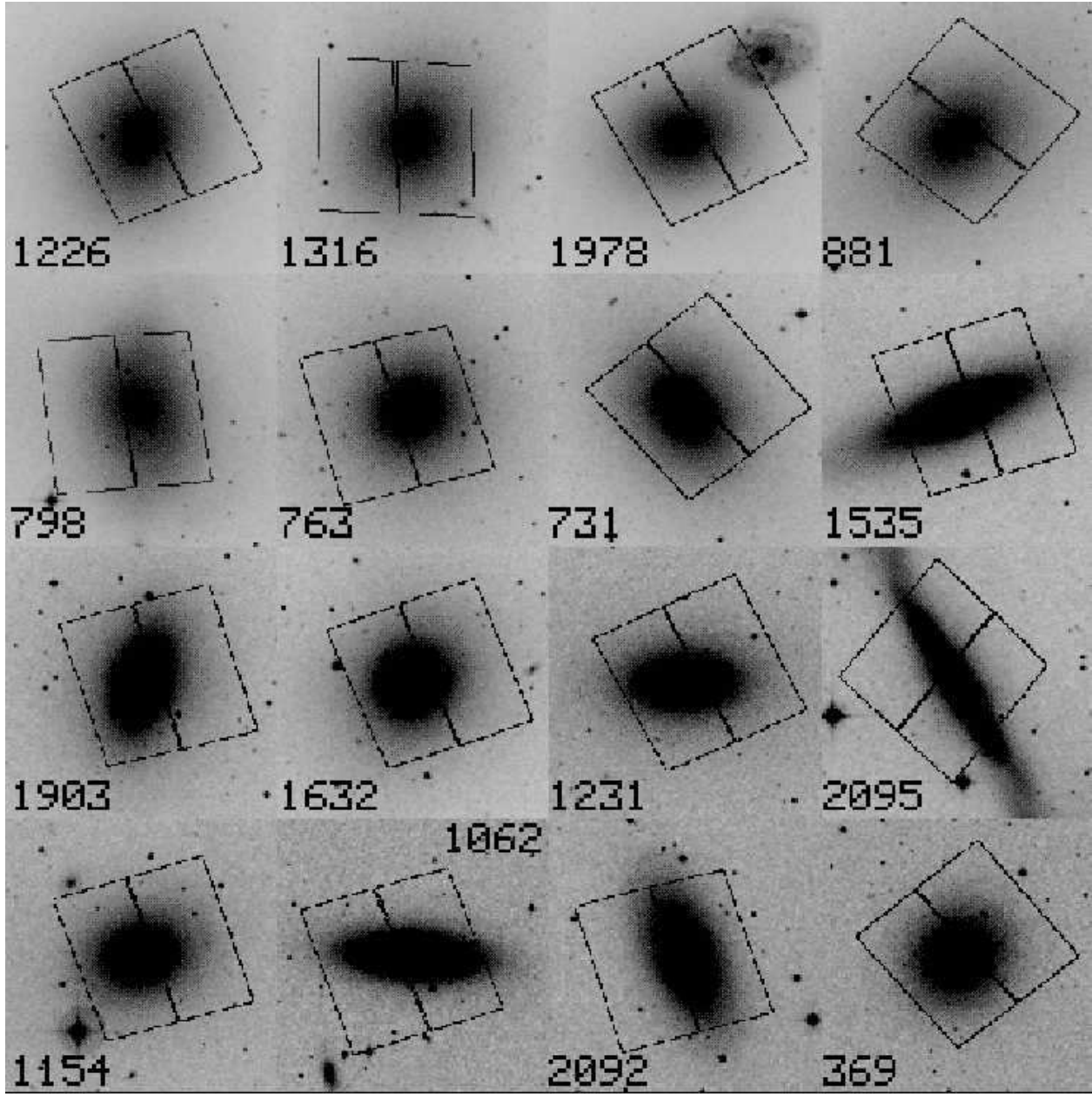
Fig. 9.— Digitized Sky Survey images for ACS Virgo Cluster Survey galaxies #1–16. Images measure $6' \times 6'$ and are oriented so that North is up and East is to the left. VCC identifications are labelled in each panel, while the overlay shows the location and orientation of the ACS/WFC field of view.
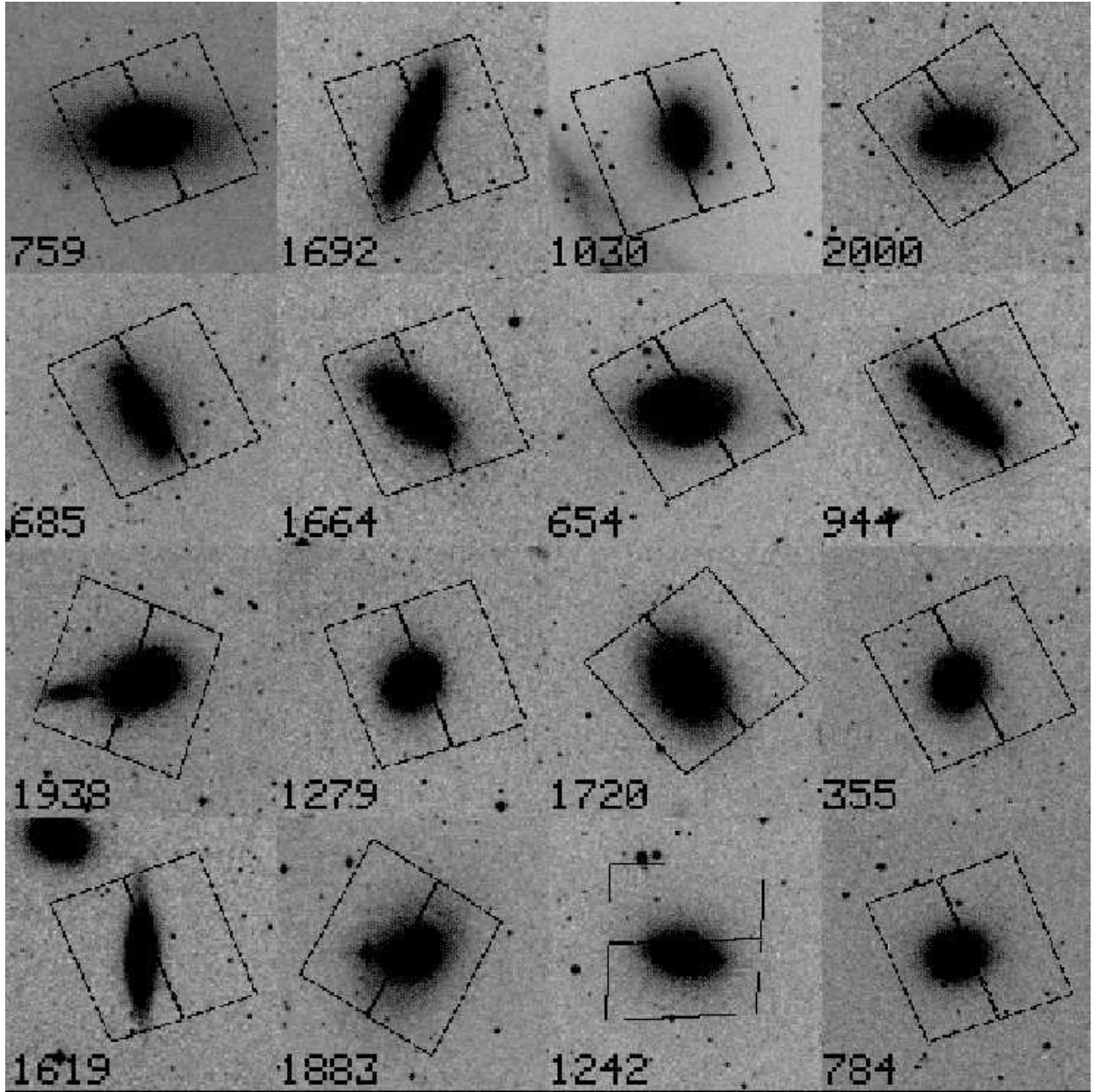
Fig. 10.— Same as Figure 9, except for galaxies #17–32.
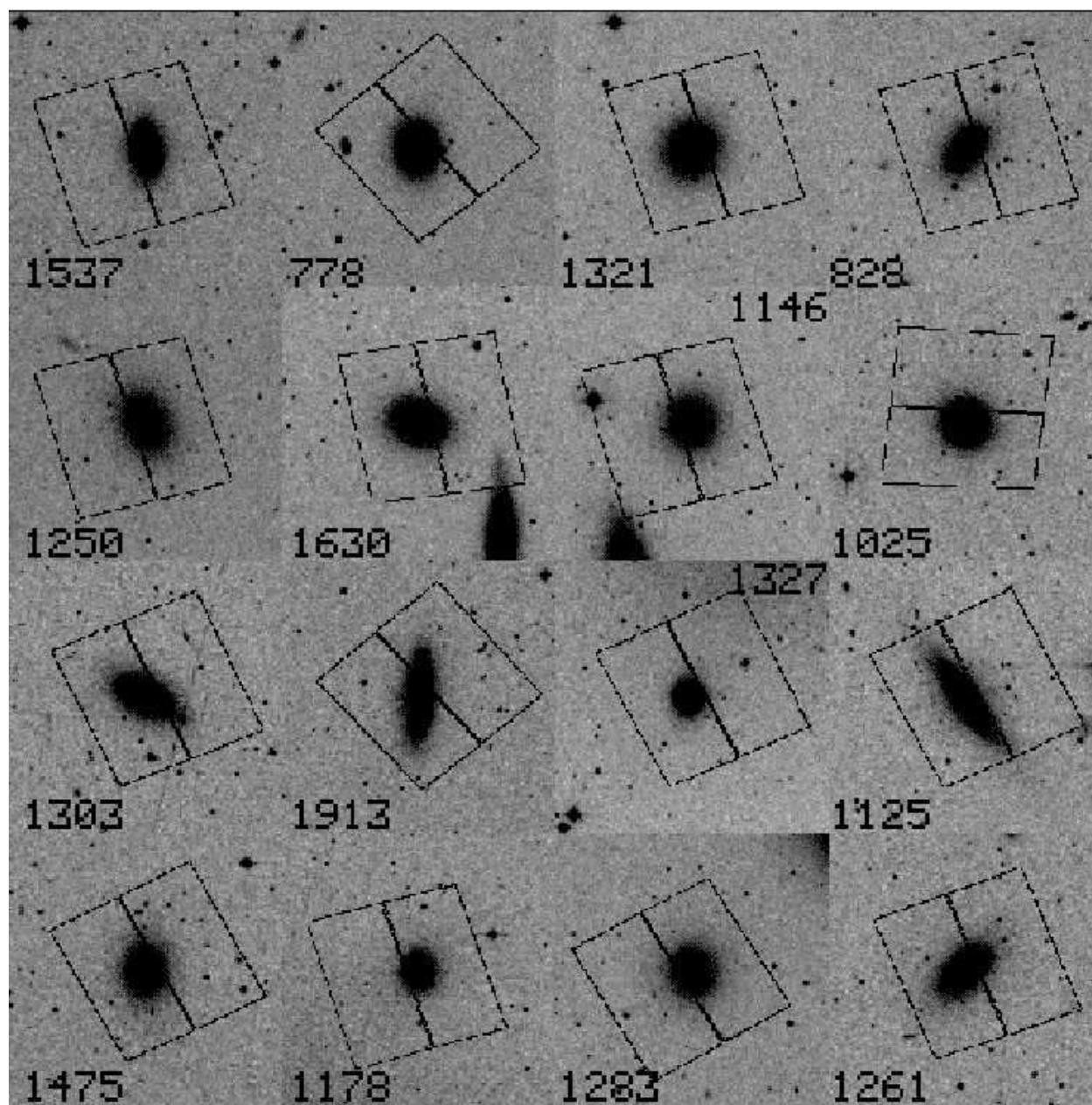
Fig. 11.— Same as Figure 9, except for galaxies #33–48.
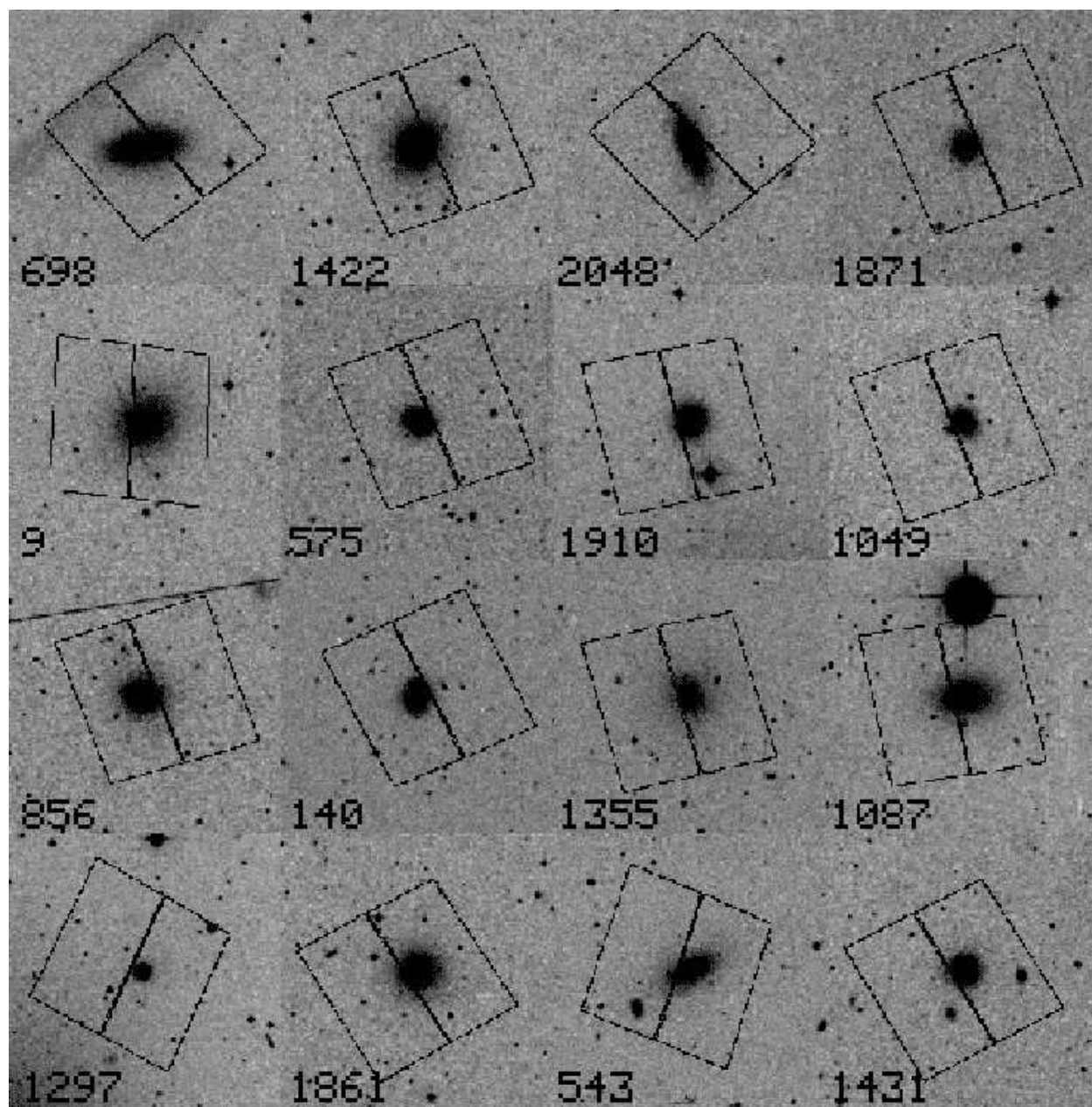
Fig. 12.— Same as Figure 9, except for galaxies #49–64.
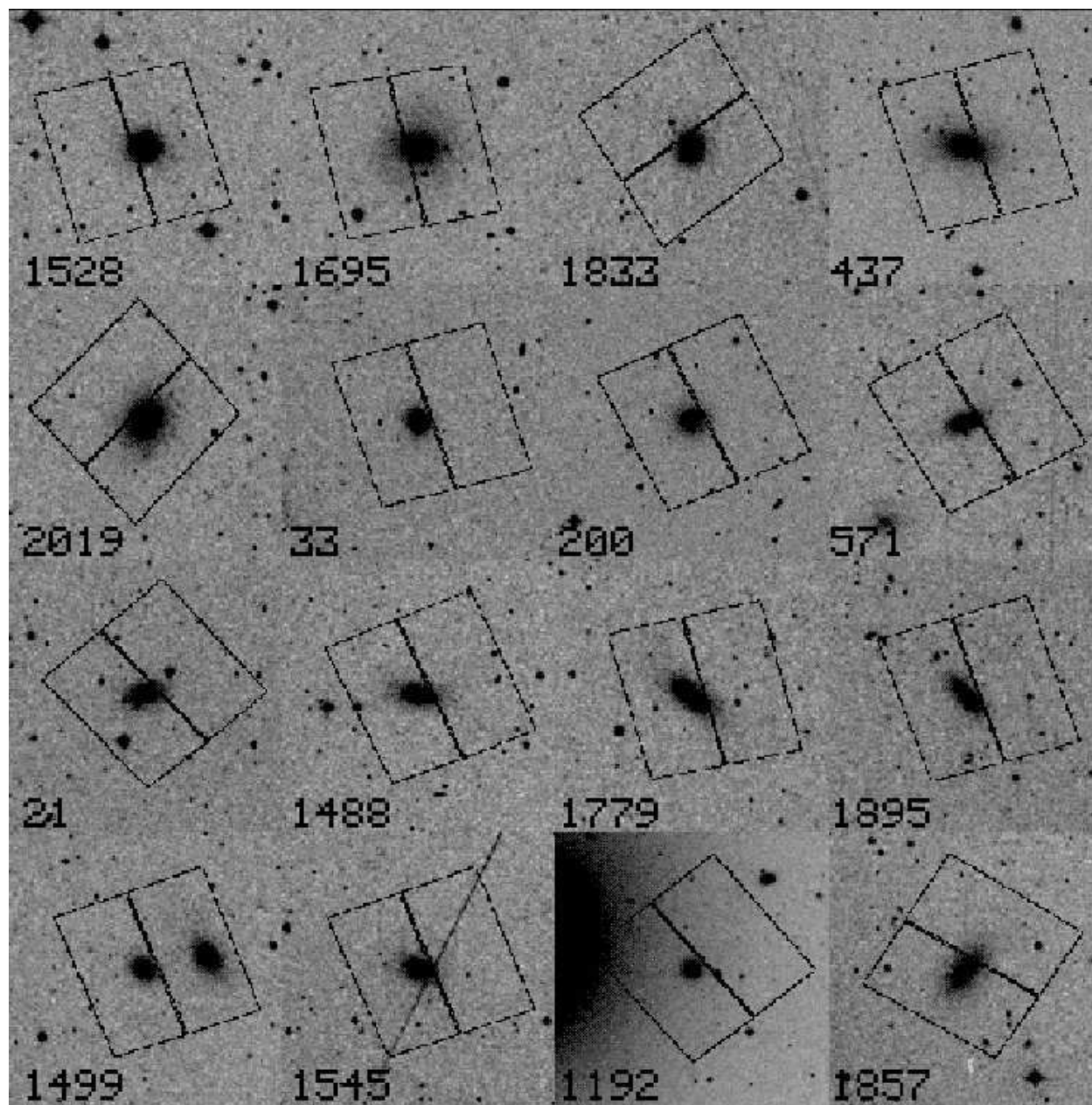
Fig. 13.— Same as Figure 9, except for galaxies #65–80.
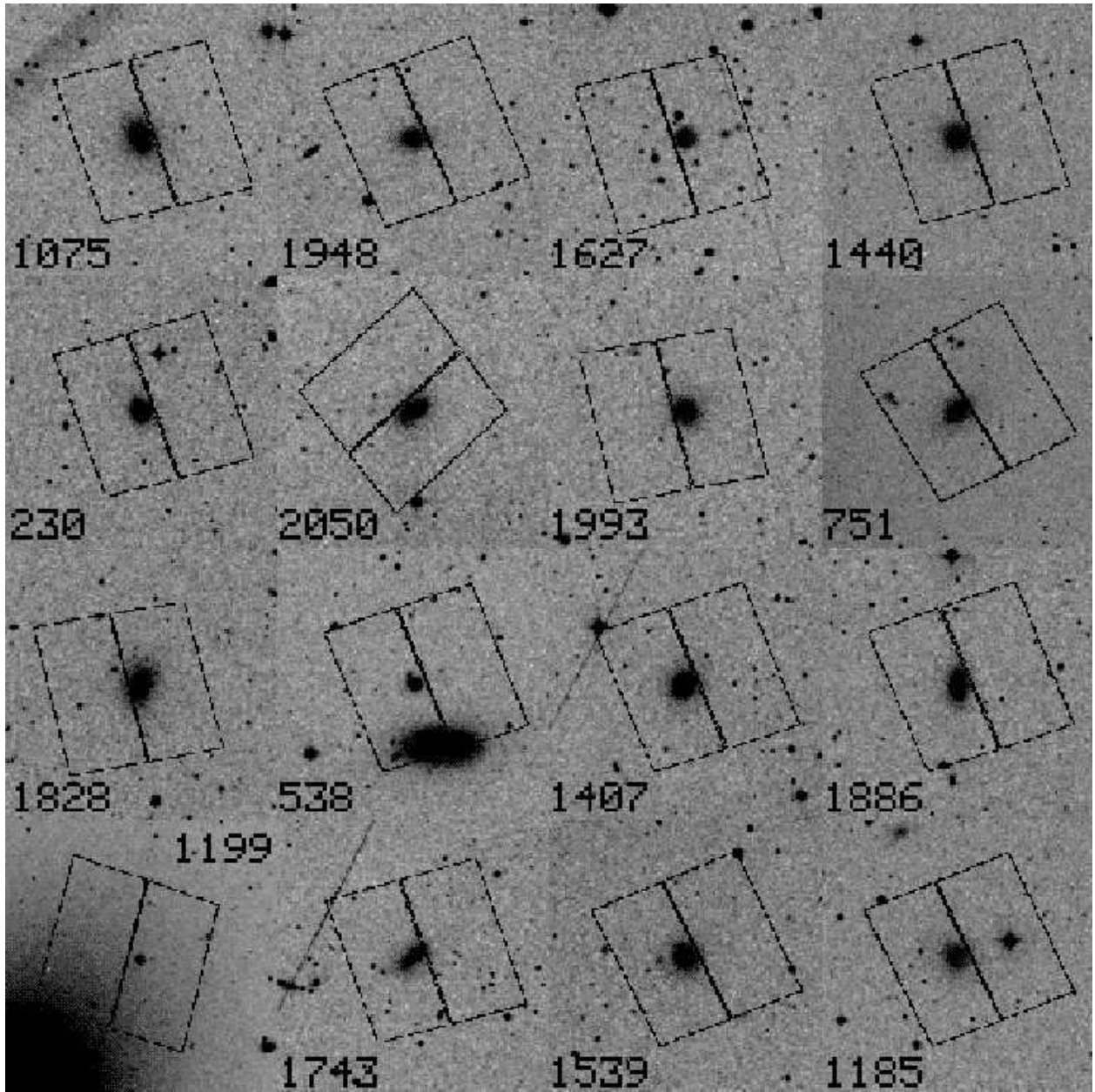
Fig. 14.— Same as Figure 9, except for galaxies #81–96.
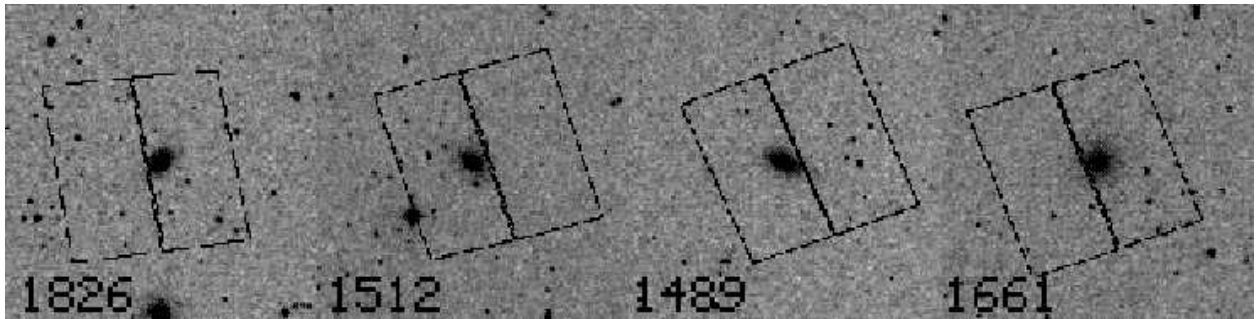
Fig. 15.— Same as Figure 9, except for galaxies #97–100.
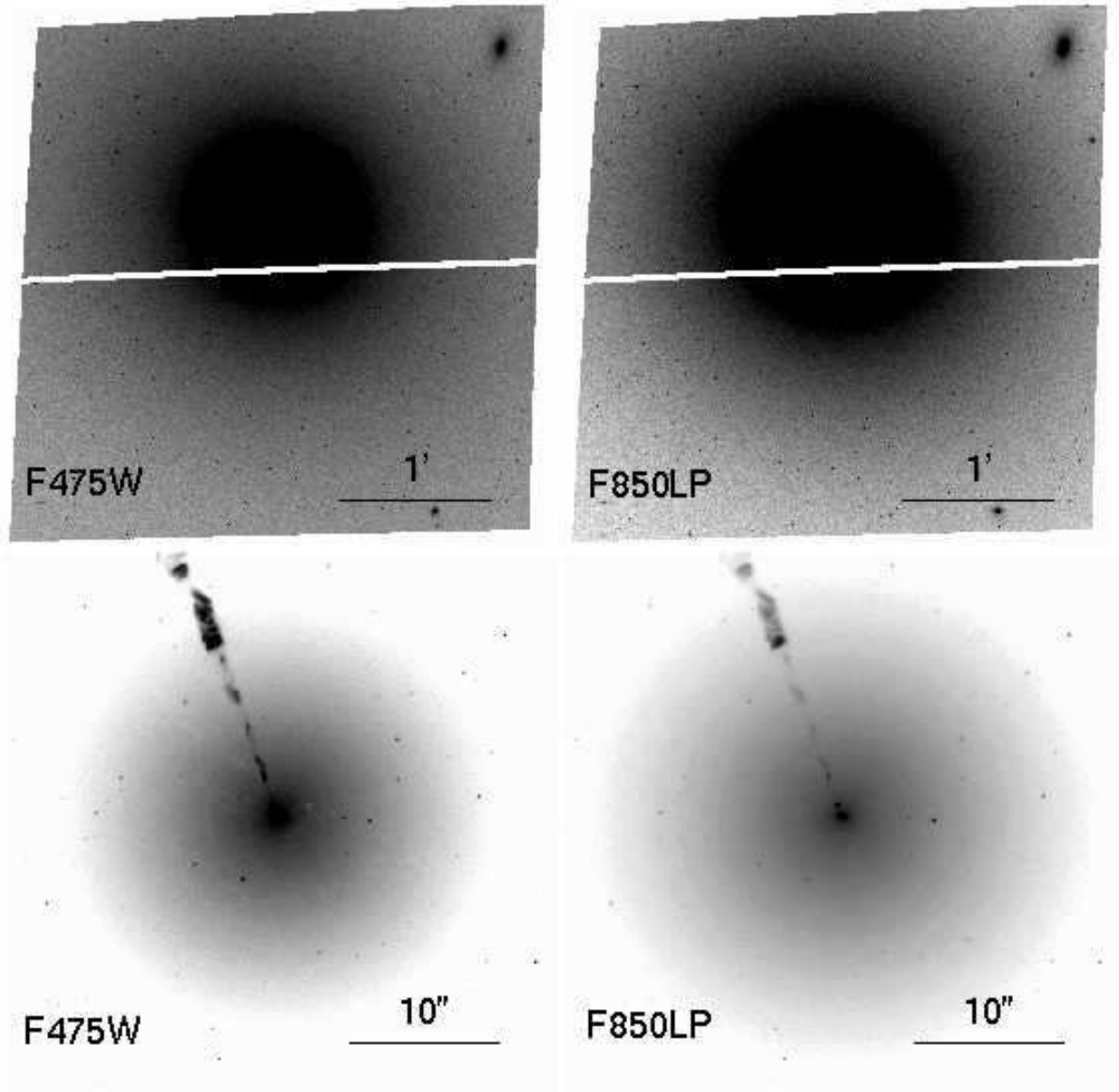
Fig. 16.— F475W and F850LP images for VCC1316 (M87). The upper panels show the full ACS/WFC images, while the bottom panels show $36'' \times 36''$ regions centered on the galaxy's nucleus.
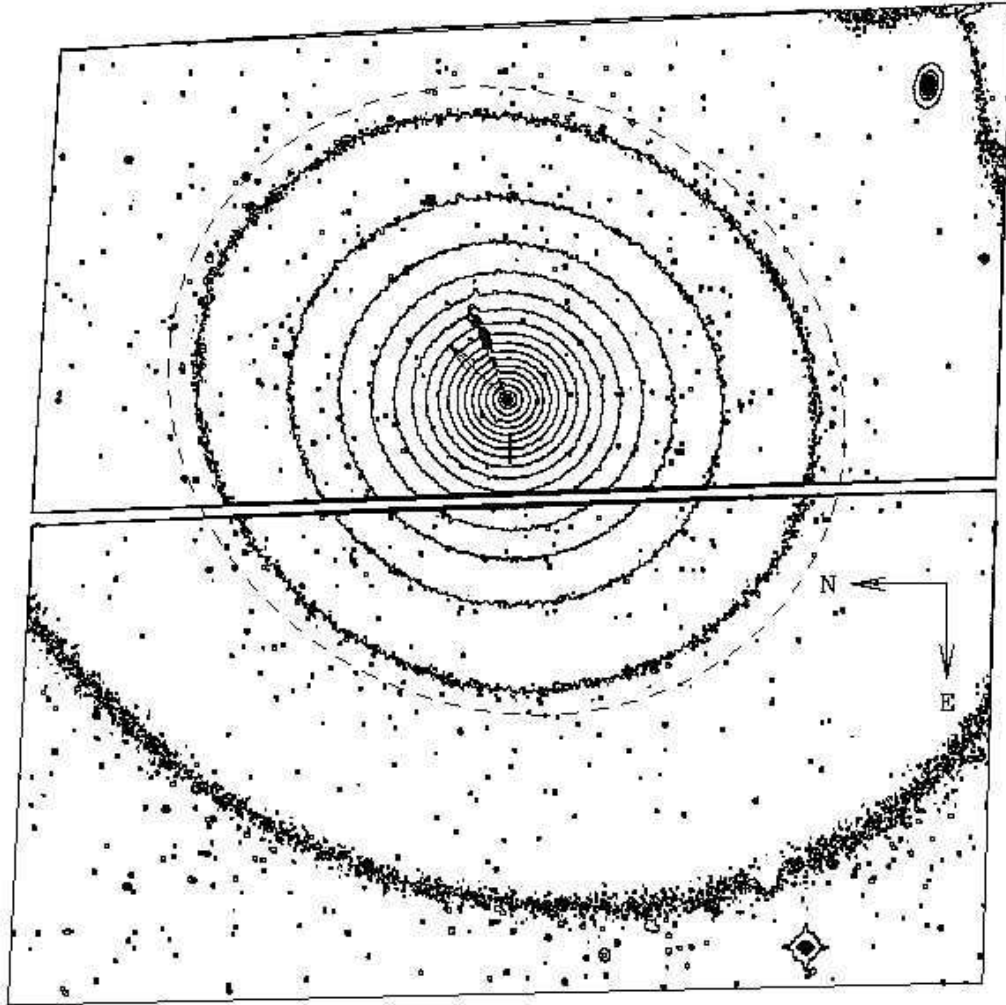
Fig. 17.— Field orientation for VCC1316 (M87). Surface brightness contours for the co-added, distortion-corrected, background-subtracted F850LP image are shown by the thin curves. The cross shows the location of the WFC aperture. The diagonal arrow indicates the direction of the WFPC2 parallel field, offset by $\approx 5\rlap{.}'8$ in the HST focal plane. The dashed curve shows the ellipse which best-fits the galaxy isophotes at a surface brightness of $\mu_z = 20$ mag arcsec^{-2}.

Table 1.   Basic Data for ACS Virgo Cluster Survey Galaxies.

ID	VCC	α (J2000)	δ (J2000)	B_T (mag)	$\langle v_r \rangle$ (km s^{-1})	Type	Other
1	1226	12:29:46.79	+08:00:01.5	9.31	997±7	E2/S0$_1$(2)	M49, N4472
2	1316	12:30:49.42	+12:23:28.0	9.58	1307±7	E0	M87, N4486
3	1978	12:43:39.66	+11:33:09.4	9.81	1117±6	S0$_1$(2)	M60, N4649
4	881	12:26:11.74	+12:56:46.4	10.06	-244±5	S0$_1$(3)/E3	M86, N4406
5	798	12:25:24.04	+18:11:25.9	10.09	729±2	S0$_1$(3) pec	M85, N4382
6	763	12:25:03.72	+12:53:13.2	10.26	1060±6	E1	M84, N4374
7	731	12:24:28.20	+07:19:03.0	10.51	1243±6	E3	N4365
8	1535	12:34:03.10	+07:41:59.0	10.61	448±8	S0$_3$(6)	N4526
9	1903	12:42:02.40	+11:38:48.0	10.76	410±6	E4	M59, N4621
10	1632	12:35:39.82	+12:33:22.6	10.78	340±4	S0$_1$(0)	M89, N4552
11	1231	12:29:48.87	+13:25:45.7	11.10	2244±2	E5	N4473
12	2095	12:52:56.00	+11:13:53.0	11.18	984±41	S0$_1$(9)	N4762
13	1154	12:29:00.03	+13:58:42.9	11.37	1210±16	S0$_3$(2)	N4459
14	1062	12:28:03.90	+09:48:14.0	11.40	532±8	SB0$_1$(6)	N4442
15	2092	12:52:17.50	+11:18:50.0	11.51	1377±15	SB0$_1$(5)	N4754
16	369	12:19:45.42	+12:47:54.3	11.80	1009±13	SB0$_1$	N4267
17	759	12:24:55.50	+11:42:15.0	11.80	943±19	SB0$_2$(r)(3)	N4371
18	1692	12:36:53.40	+07:14:47.0	11.82	1730±13	S0$_1$(7)/E7	N4570
19	1030	12:27:40.49	+13:04:44.2	11.84	801±10	SB0$_1$(6)	N4435
20	2000	12:44:31.95	+11:11:25.1	11.94	1083±4	E3/S0$_1$(3)	N4660
21	685	12:23:57.90	+16:41:37.0	11.99	1241±19	S0$_1$(8)	N4350
22	1664	12:36:26.86	+11:26:20.6	12.02	1142±2	E6	N4564
23	654	12:23:35.28	+16:43:22.3	12.03	950±9	RSB0$_2$(5)	N4340
24	944	12:26:50.53	+09:35:02.0	12.08	843±15	S0$_1$(7)	N4417
25	1938	12:42:47.40	+11:26:33.0	12.11	1164±10	S0$_1$(7)	N4638
26	1279	12:30:17.39	+12:19:43.9	12.15	1349±3	E2	N4478
27	1720	12:37:30.61	+09:33:18.8	12.29	2273±12	S0$_{1/2}$(4)	N4578
28	355	12:19:30.61	+14:52:41.4	12.41	1359±4	SB0$_{2/3}$	N4262
29	1619	12:35:30.61	+12:13:15.4	12.50	381±9	E7/S0$_1$(7)	N4550
30	1883	12:41:32.70	+07:18:53.0	12.57	1875±22	RSB0$_{1/2}$	N4612
31	1242	12:29:53.49	+14:04:07.0	12.60	1609±11	S0$_1$(8)	N4474
32	784	12:25:14.75	+15:36:27.2	12.67	1069±10	S0$_1$(2)	N4379
33	1537	12:34:06.10	+11:19:17.0	12.70	1374±10	SB0$_2$(5)	N4528
34	778	12:25:12.27	+14:45:43.8	12.72	1375±11	S0$_1$(3)	N4377
35	1321	12:30:52.21	+16:45:32.6	12.84	967±6	S0$_1$(1)	N4489
36	828	12:25:41.70	+12:48:38.0	12.84	561±15	E5	N4387
37	1250	12:29:59.10	+12:20:55.0	12.91	1970±11	S0$_3$(5)	N4476
38	1630	12:35:37.97	+12:15:50.5	12.91	1172±6	E2	N4551
39	1146	12:28:57.56	+13:14:30.8	12.93	635±6	E1	N4458
40	1025	12:27:36.71	+08:09:14.8	13.06	1071±6	E0/S0$_1$(0)	N4434
41	1303	12:30:40.64	+09:00:55.9	13.10	875±10	SB0$_1$(5)	N4483
42	1913	12:42:10.70	+07:40:37.0	13.22	1892±37	E7	N4623
43	1327	12:30:57.56	+12:16:17.2	13.26	150±45	E2	N4486A
44	1125	12:28:43.37	+11:45:21.0	13.30	195±47	S0$_1$(9)	N4452
45	1475	12:33:04.95	+16:15:55.9	13.36	951±11	E2	N4515

Table 1—Continued

ID	VCC	α (J2000)	δ (J2000)	B_T (mag)	$\langle v_r \rangle$ (km s^{-1})	Type	Other
46	1178	12:29:21.30	+08:09:23.0	13.37	1243±2	E3	N4464
47	1283	12:30:18.40	+13:34:40.9	13.45	876±10	SB0$_2$(2)	N4479
48	1261	12:30:10.39	+10:46:46.1	13.56	1871±16	d:E5,N	N4482
49	698	12:24:05.00	+11:13:06.0	13.60	2080±10	S0$_1$(8)	N4352
50	1422	12:32:14.21	+10:15:05.0	13.64	1288±10	E1,N:	I3468
51	2048	12:47:15.32	+10:12:13.0	13.81	1084±12	d:S0(9)	I3773
52	1871	12:41:15.72	+11:23:13.5	13.86	567±10	E3	I3653
53	9	12:09:22.34	+13:59:33.1	13.93	1804±49	dE1,N	I3019
54	575	12:22:43.31	+08:11:53.7	14.14	1231±9	E4	N4318
55	1910	12:42:08.69	+11:45:14.9	14.17	206±26	dE1,N	I809
56	1049	12:27:54.86	+08:05:25.2	14.20	716±36	S0(4)	U7580
57	856	12:25:57.81	+10:03:12.8	14.25	1025±10	dE1,N	I3328
58	140	12:15:12.58	+14:25:59.1	14.30	1072±46	S0$_{1/2}$(4)	I3065
59	1355	12:31:20.04	+14:06:53.5	14.31	1332±63[a]	dE2,N	I3442
60	1087	12:28:14.90	+11:47:24.0	14.31	675±12	dE3,N	I3381
61	1297	12:30:31.85	+12:29:26.0	14.33	1555±4	E1	N4486B
62	1861	12:40:58.54	+11:11:04.4	14.37	470±39	dE0,N	I3652
63	543	12:22:19.55	+14:45:38.6	14.39	985±12	dE5	U7436
64	1431	12:32:23.37	+11:15:46.2	14.51	1500±38	dE0,N	I3470
65	1528	12:33:51.62	+13:19:21.3	14.51	1608±35	d:E1	I3501
66	1695	12:36:54.87	+12:31:12.5	14.53	1547±29	dS0:	I3586
67	1833	12:40:19.65	+15:56:07.2	14.54	1679±34	S0$_1$(6)	
68	437	12:20:48.82	+17:29:13.4	14.54	1474±46	dE5,N	U7399A
69	2019	12:45:20.42	+13:41:33.0	14.55	1895±44	dE4,N	I3735
70	33	12:11:07.76	+14:16:29.8	14.67	1093±52	d:E2,N:	I3032
71	200	12:16:33.68	+13:01:53.1	14.69	65±43	dE2,N	
72	571	12:22:41.14	+07:57:01.1	14.74	1047±37	SB0$_1$(6)	
73	21	12:10:23.19	+10:11:17.6	14.75	506±35	dS0(4)	I3025
74	1488	12:33:13.44	+09:23:49.8	14.76	1157±48	E6:	I3487
75	1779	12:39:04.67	+14:43:51.5	14.83	1313±45	dS0(6):	I3612
76	1895	12:41:52.00	+09:24:10.3	14.91	1032±51	d:E6	U7854
77	1499	12:33:19.79	+12:51:12.8	14.94	-575±35	E3 pec or S0	I3492
78	1545	12:34:11.54	+12:02:55.9	14.96	2050±32	E4	I3509
79	1192	12:29:30.20	+07:59:34.0	15.04	1426±22	E3	N4467
80	1857	12:40:53.10	+10:28:34.0	15.07	634±69	dE4:,N?	I3647
81	1075	12:28:12.29	+10:17:51.0	15.08	1844±40	dE4,N	I3383
82	1948	12:42:58.02	+10:40:54.5	15.10	1672±98	dE3	
83	1627	12:35:37.25	+12:22:54.9	15.16	236±41	E0	
84	1440	12:32:33.39	+15:24:55.2	15.20	414±44	E0	I798
85	230	12:17:19.64	+11:56:36.2	15.20	1490±65	dE4:,N:	I3101
86	2050	12:47:20.69	+12:09:58.7	15.20	1193±48	dE5:,N	I3779
87	1993	12:44:12.02	+12:56:30.1	15.30	875±50	E0	
88	751	12:24:48.34	+18:11:42.0	15.30	710±39	dS0	I3292
89	1828	12:40:13.38	+12:52:29.0	15.33	1517±57	dE2,N	I3635
90	538	12:22:14.83	+07:10:00.8	15.40	500±50	E0	N4309A

Table 1—Continued

ID	VCC	α (J2000)	δ (J2000)	B_T (mag)	$\langle v_r \rangle$ (km s^{-1})	Type	Other
91	1407	12:32:02.69	+11:53:24.8	15.49	1001±11	dE2,N	I3461
92	1886	12:41:39.41	+12:14:52.4	15.49	1159±65	dE5,N	
93	1199	12:29:34.97	+08:03:31.4	15.50	900±50	E2	
94	1743	12:38:06.77	+10:04:56.6	15.50	1279±10	dE6	I3602
95	1539	12:34:06.77	+12:44:30.1	15.68	1390±50	dE0,N	
96	1185	12:29:23.43	+12:27:02.4	15.68	500±50	dE1,N	
97	1826	12:40:11.24	+09:53:45.9	15.70	2033±38	dE2,N	I3633
98	1512	12:33:34.56	+11:15:42.8	15.73	762±35	dS0 pec	
99	1489	12:33:13.84	+10:55:43.6	15.89	80±50	dE5,N?	I3490
100	1661	12:36:24.81	+10:23:04.6	15.97	1400±50	dE0,N	

[a]Velocity from Binggeli, Popescu & Tammann (1993). Note that Karachentsev & Karachentsev (1982) claim a (heliocentric) velocity of $\langle v_r \rangle = 6210 \pm 60$ km s^{-1}.

Note. — Units of right ascension are hours, minutes, and seconds, and units of declination are degrees, arcminutes, and arcseconds.

Table 2.   Morphologies of ACS Virgo Cluster Survey Galaxies.

Type	Number
E	26
E/S0	7
S0	32
dE	5
dE,N	24
dS0	6
All	100